NOTE TO USERS

Université d'Ottawa · University of Ottawa

Université d'Ottawa · University of Ottawa

FACULTÉ DES ÉTUDES SUPÉRIEURES ET POSTDOCTORALES

FACULTY OF GRADUATE AND POSTDOCTORAL STUDIES

Salvador REGO BARCENA

AUTEUR DE LA THÈSE - AUTHOR OF THESIS

M. A. Sc. (Electrical Engineering)

GRADE - DEGREE

School of Information, Technology and Engineering

FACULTÉ, ÉCOLE, DÉPARTEMENT - FACULTY, SCHOOL, DEPARTMENT

TITRE DE LA THÈSE - TITLE OF THE THESIS

Design and Performance of a Coil Heat Exchanger for Thermal Recovery from Solution Gas Flares

J. Thibault

DIRECTEUR DE LA THÈSE - THESIS SUPERVISOR

D. Taylor

CO-DIRECTEUR DE LA THÈSE - THESIS CO-SUPERVISOR

EXAMINATEURS DE LA THÈSE - THESIS EXAMINERS

D. McLean

A. Y. Tremblay

J.-M. De Koninck, Ph.D.

LE DOYEN DE LA FACULTÉ DES ÉTUDES SUPÉRIEURES ET POSTDOCTORALES

DEAN OF THE FACULTY OF GRADUATE AND POSTDOCTORAL STUDIES

DESIGN AND PERFORMANCE OF A COIL HEAT EXCHANGER FOR THERMAL RECOVERY FROM SOLUTION GAS FLARES

By

SALVADOR REGO BÁRCENA

A thesis submitted to the Faculty of Graduate and Postdoctoral Studies in partial fulfillment of the requirements for the degree of

Master of Applied Science

In

Department of Chemical Engineering
University of Ottawa.

Your file Votre référence
ISBN: 0-494-01590-X
Our file Notre référence
ISBN: 0-494-01590-X

ABSTRACT

Solution gas is commonly evolved in the production of oil and bitumen. When crude oil in the reservoir is exposed to atmospheric pressure, the gaseous stream dissolved in the liquid phase comes out of solution. Flaring or venting directly to the atmosphere are two common means to dispose of solution gas at oil and bitumen batteries where it cannot be conserved. Although the trend for conservation continues to grow, there were still 408 million m^3 of solution gas flared and 435 million m^3 vented in 2003 at crude oil and bitumen batteries in Alberta, Canada. Our project aims at the partial recovery of the heat that is currently lost to the atmosphere when solution gas burns in an open-air flame. The ultimate objective of the recovery system is the generation of electricity to inject enough air for the complete combustion of solution gas that is flared in order to reduce greenhouse gas emissions and smoke formation.

In the proposed system, the flame is enclosed so that a stream of oil extracts energy from the flue gas in a counter-current, coil heat exchanger (CHE) placed on top of the stack. The oil temperature must rise from 123°C to 180°C to provide the specified heat load (69.6 kW) to the boiler of a commercial Organic Rankine Engine where 7.52 kW of electricity is produced. In the reference case, solution gas is modelled as a stream of pure methane gas (CH_4) at STP that reacts with air in a burner. The nominal flow rate of methane is 21 kg/h (257 070 m^3/year), which is similar to the mean volume flared or vented at all physical batteries in Alberta in 1999 (246 900 m^3/year). Combustion air is supplied 25% in excess of the stoichiometric amount. The mass flow rate of flue gas is 0.1307 kg/s. A flue gas temperature of 1300°C was assumed to account for heat losses between the burner and the ambient air.

Geometry and choice of materials for the energy recovery system are addressed. A simple, steady-state model is presented for the calculation of the required surface area of the coiled tube. The model is based on the thermal circuit among the flue gas, the oil and the ambient air, and accounts for heat losses. Meanwhile, the CHE is divided into cylindrical control volumes (CV) containing one full turn of the coiled tube. The thermal circuit for each CV is solved by an implicit technique allowing for easy visualisation of key parameters (temperature, thermal resistance and heat flow) along the CHE. Results show that heat

transfer to the oil is controlled by gas side processes (convection and radiation). The outer surface area of the coiled tube is 1.181 m^2, setting the height of the CHE at 1.23 m. Losses are minimised by 1.27 cm of refractory fibre insulation around the 25.4 cm ID stack. The model was computerized in order to extend the solution of the design and performance problems of the CHE to other flue gas conditions (mass flow rate and inlet temperature).

RÉSUMÉ

Les gaz de solution sont communément libérés lors de l'extraction de pétrole et du bitume lorsqu'ils sont exposés à pression atmosphérique. Brûler dans une cheminée ou décharger directement à l'atmosphère sont deux manières utilisées pour se débarrasser de la partie excédentaire des gaz dégagés lors de la récupération et du transport du pétrole et du bitume. Bien que la tendance pour la conservation continue à augmenter, il n'en demeure pas moins que 408 millions de m^3 de gaz ont été brûlés et 435 millions de m^3 déchargés directement à l'atmosphère en 2003 pour les puits de pétrole brut et de bitume de la province de l'Alberta au Canada. Ce projet vise la récupération partielle de l'énergie qui est présentement perdue à l'atmosphère lorsque les gaz sont brûlés dans une flamme à l'air libre. L'objectif ultime du système de récupération d'énergie est la production d'électricité pour permettre l'injection d'une quantité d'air suffisante pour la combustion complète des gaz rejetés et ainsi réduire les émissions de gaz à effet de serre et la fumée.

Dans le système proposé, la flamme se retrouve à l'intérieur de la cheminée de sorte qu'une quantité d'énergie peut être récupérée par un courant d'huile caloporteur circulant dans un échangeur de chaleur en spirale situé dans la partie supérieure de la cheminée. La température de l'huile doit augmenter de 123°C à 180°C pour fournir un flux thermique de 69.6 kW à un système commercial utilisant un cycle de Rankine pour générer 7.52 kW d'électricité. Dans le cas de référence, on suppose que les gaz rejetés sont constitués d'un courant de méthane pur (CH_4) à STP qui réagit avec de l'air dans un brûleur. Le débit nominal du méthane est 21 kg/h (257 070 m^3/an), ce qui s'apparente au volume moyen de gaz rejetés de tous les postes de récupération de l'Alberta en 1999 (246 900 m^3/an). L'air de combustion est fourni à raison de 25% excédentaire par rapport à la quantité

stœchiométrique. Le débit massique des gaz de combustion est de 0.1307 kg/s. Une température des gaz d'échappement de 1300°C est supposée pour prendre en compte les pertes d'énergie.

La géométrie et le choix des matériaux pour l'échangeur de chaleur sont présentés. Un modèle simple en régime stationnaire est développé pour calculer la surface requise pour l'échangeur de chaleur. Le modèle représente en détail les échanges thermiques entre les gaz de combustion, le liquide caloporteur et le milieu ambiant. Pour solutionner ce problème, l'échangeur de chaleur est divisé en volumes de contrôle cylindriques (CV) équivalant à un tour complet du tube de l'échangeur de chaleur. Le bilan thermique de chaque CV est résolu par une technique implicite permettant de suivre l'évolution des variables principales (température, résistance thermique et flux de chaleur) le long de l'échangeur. Les résultats montrent que le transfert thermique vers le liquide caloporteur est contrôlé par le transfert de chaleur du côté des gaz de combustion (convection et rayonnement). La surface externe de la bobine de l'échangeur de chaleur est de 1.181 m^2 pour une longueur de 1.23 m. Les pertes de chaleur ont été réduites par l'utilisation d'une couche de 1.27 cm d'isolant réfractaire autour de la cheminée ayant un diamètre de 25.4 cm. Le modèle a été conçu pour permettre d'étudier ce système sous diverses conditions opératoires.

ACKNOWLEDGEMENTS

This work was commissioned by the Advanced Combustion Technologies Group at the CANMET Energy Technology Centre (Natural Resources Canada) through the efforts of Dr. Peter Gogolek, Project Leader of the Flare Test Facility. I would like to thank Dr. Gogolek for his valuable assistance throughout this project.

I am grateful to my two co-supervisors: Dr. David Taylor (Chemical Eng.), whose dedication to teaching motivated me to pursue graduate studies at the University of Ottawa, and with the encouragement and discipline of Dr. Jules Thibault (Chemical Eng.), I was able to complete this project and present it successfully at local and international conferences.

Flaring in Alberta was demystified with the help of Dr. Matthew Johnson (Mechanical Eng.) and his previous work at the University of Alberta. The seed of the structure for the heat transfer model is based on several conversations with Dr. Boguslaw Kruczek (Chemical Eng.). It was a pleasure to work with him as a Teaching Assistant. To Dr. William Hallett (Mechanical Eng.) I owe the satisfaction of working as an engineer and his suggestion for my future studies at the University of Toronto. Dr. Miguel Rodriguez (Biochemistry) has been a great source of inspiration throughout my six years in Ottawa.

I would like to thank fellow graduate students Marc Laplante, Hayley Halsall-Whitney, Rafi Chapanian and Arden Tuck for their support and friendship.

This thesis is dedicated to my parents, Juan Ramón and María del Carmen.

NOMENCLATURE

Notation

A_{co}	outer surface area of the coil [m^2]
b	coil pitch ("height of one turn") [m]
C_P	heat capacity at constant pressure [J/kg^{o}C]
CV	control volume
D	diameter [m]
E	blackbody emissive power [W/m^2]
F	view factor
G	radiation incident on a surface ("irradiation") [W/m^2]
H	height of the Coil Heat Exchanger [m]
h	heat transfer coefficient [$W/m^{2o}C$]
J	radiation leaving a surface ("radiosity") [W/m^2]
L	coiled tube length [m]
L_m	mean beam length of the gas in the CV [m]
l_{turn}	length of one turn of coiled tube (= $2\pi R_c$) [m]
M	mass flow rate [kg/s]
N	total number of CV into which the Coil Heat Exchanger is divided
P	total pressure [atm]
P_{rad}	sum of the partial pressure of water vapour and carbon dioxide in the flue gas [atm]
p	partial pressure [atm]
q	heat flux [W/m^2]
Q	heat flow rate [W]
R	resistance to heat transfer [^{o}C/W]
R_c	radius of curvature of the coiled tube [m]
T	temperature [^{o}C]
u	average bulk velocity [m/s]

Greek Letters (in order of appearance in text)

λ_A	stoichiometric number (= actual air/stoichiometric air, by vol.)
Δx	length of the coiled tube in a CV [m]
Δy	height of the CV [m]
λ	thermal conductivity [W/m °C]
η	dynamic viscosity [kg/m·s]
ν	kinematic viscosity [m^2/s]
β	relaxation coefficient, see (2.70)
γ	under-relaxation coefficient, see (2.71)
$\alpha, \varepsilon, \tau$	absorptivity, emissivity and transmissivity of the flue gas
ε_c	emissivity of the coiled tube

Subscripts

c	coiled tube
e	environment
f	flue gas
H, L	high and low reference temperatures, see Eq. (2.41) through Eq. (2.45)
o	oil
s	stack
cc, cs, sc, ss	view factor identifiers between the coiled tube (c) and the stack (s), see Eq. 2.28 through Eq. 2.30
ci	internal convection of the oil relative to the coiled tube
cl	client
co	external convection of the flue gas relative to the coiled tube
fc	from the flue gas to the coiled tube
fs	from the flue gas to the stack
ins	insulating material
jack	weather jacket
rc	radiation to the coiled tube
si	internal convection of the flue gas relative to the insulated stack
so	external convection of the outdoors air relative to the insulated stack
f∞	mainstream velocity of the flue gas in an empty stack
1, 2, 3, 4	surface identifiers

Superscripts

*	guessed value

TABLE OF CONTENTS

LIST OF TABLES

LIST OF FIGURES

1 Introduction

1.1 Handling of Solution Gas in Alberta

Solution gas is commonly evolved in the production of oil and bitumen. When crude oil in the reservoir is exposed to atmospheric pressure, the gaseous stream dissolved in the liquid phase comes out of solution. The liquid phase is an emulsion of oil and water. Solution gas typically contains light hydrocarbons (methane, ethane, etc.), inert compounds (carbon dioxide, nitrogen) and toxic species (hydrogen sulphide). The level of hydrogen sulphide (H_2S) is normally used to label solution gas either as "sweet" (for concentrations of H_2S less than 10 ppm by volume) or "sour" (for concentrations larger than 10 ppm). Since the separation from the liquid phase at a battery site may not be complete, some liquid droplets (heavier hydrocarbons and brackish water) are likely to be entrained in solution gas.

Solution gas is most often conserved and processed as sales-grade natural gas. The level of solution gas conserved in the province of Alberta (Canada) has increased almost continuously from 90.2% in 1993 to 95.4% in 2003 (AEUB, 2004). In 2003, operators in Alberta produced 18 326 million cubic meters (m^3) of solution gas and conserved 17 483 million m^3 (see data from AEUB, 2004).

In cases where conservation is uneconomical or the specific energy content of solution gas is too low, gas is flared or vented. Flaring is the disposal of unwanted gaseous species via combustion in an open-air flame. Venting is the direct release of these gases to the atmosphere. Flaring and venting pose environmental, health and thus, public opinion problems. From the environmental angle, flaring is preferred over venting inasmuch as the global warming potential of methane (the most common species in solution gas) is twenty-three times larger than that of carbon dioxide by mass (IPCC, 2001). The concern of methane emissions to the environment also exists when the combustion efficiency of a flare drops due to increasing crosswind speed or reduced energy content (Johnson and Kostiuk, 2002; Gogolek and Hayden, 2002). Smoke formation in flares generates negative public opinion. However, techniques such as water or steam injection that suppress this problem are well known (Brzustowski, 1976).

Flaring and venting of solution gas in Alberta have decreased almost continuously from 2016 million m^3 in 1993 to 843 million m^3 in 2003 (AEUB, 2004). In 2003, oil and bitumen batteries in Alberta flared 408 million m^3 of solution gas. Other sources of solution gas flaring are well tests, gas-gathering systems, gas plants and gas batteries (AEUB, 2004). Interestingly the Alberta Energy and Utilities Board (AEUB) does not include solution gas volumes from these sources in the flared or vented category (see Figures 1, 2 and 3 in AEUB, 2004) indicating that solution gas conservation only occurs at oil or bitumen sites. Other sources (e.g., well tests) flare and vent solution gas as part of their processes or in emergency situations.

Flaring and venting in Alberta are regulated by the AEUB, an independent board that regulates the responsible development of Alberta's energy resources (oil, natural gas, oil sands, coal, and electrical energy) including pipelines and transmission lines. The AEUB also regulates investor-owned natural gas, electric, and water utilities and certain municipally owned electric utilities to ensure that customers receive reliable service at reasonable rates. The board plays an important role in collecting and distributing energy information (e.g., monthly volumes of solution gas flared or vented).

Johnson et al. (2001) presented the most comprehensive work of characterizing solution gas volumes and composition in Alberta to date using AEUB data from 1999. In total 4499 oil and bitumen batteries reported flaring and/or venting with a combined gas volume of 1423 million m^3. The distribution of annual volumes of solution gas flared or vented at physical sites was highly skewed with a mean volume of 246 900 m^3/year and a median volume of 58 700 m^3/year. Thus the largest 20% of batteries (881 sites) flared or vented nearly 60% of the solution gas flared or vented at oil and bitumen batteries in Alberta. A second interesting conclusion is the realization that larger sites tend to be more "steady", i.e., have less monthly variation in the volume of solution gas flared or vented. Just over 40% of sites had monthly deviations of 100% or less from the average volume. This property is useful when implementing alternatives to flaring and venting that rely on a steady supply of solution gas. Because of these two findings, Johnson et al. concluded "if one were to attempt

to mitigate flaring, significant progress could be made by starting with only the largest sites" (2001).

At present the AEUB does not require operators to report the composition of solution gas flared or vented at battery sites. Thus the only information available is from voluntary reporting of well tests by the operators. Gas compositions from well tests may not be representative of the gas flared or vented at battery sites, which typically collect solution gas from several wells. From the well test analyses received by the AEUB it is apparent that the main components of solution gas are light hydrocarbons. However the level of inert compounds and hydrogen sulphide can be significant at times (Johnson et al., 2001).

1.2 Alternatives to Flaring and Venting

More than 95% of the solution gas in Alberta was conserved in 2003 (see Section 1.1). The decision of whether to conserve or flare solution gas in this province is part of the flare management framework administered by the AEUB. Their policy objective hierarchy for flaring can be summarized as eliminate flaring, reduce flaring, and improve the efficiency of flares (see AEUB, 1999; a new draft version of Guide 60 released in January 2003 is currently under stakeholder consultation). The AEUB stipulates that gas must be conserved if conservation is determined to be economic according to the economic decision process detailed in Guide 60. Conservation can be achieved by directing solution gas to a gathering system. Alternatives to gas conservation include power generation (e.g., with microturbines that use natural gas) and injection into a gas pool or water disposal well. Holford and Hettiaratchi (1998) presented an initial analysis of the economics of these alternatives in the context of Alberta.

One of the proposed changes in the draft version of Guide 60 (January 2003) is that combustion of solution gas in incinerators or other types of enclosed burners would be considered as flaring instead of an alternative to conservation. Since the heat recovery system that is presented in this work requires the use of an enclosed burner for the purposes

of producing electricity (see §1.3), it remains to be seen if the recovery system will be regarded as an alternative to gas conservation.

1.3 Introducing the Heat Recovery Unit

Operators in Alberta already practice heat recovery at the battery level. In large sites the water and oil emulsion from the oil well is broken in a "treater" vessel by raising the temperature to 60°C. The heat from the hot oil effluent is sometimes transferred to the cool emulsion entering the treater.

The present work suggests partially capturing the thermal energy from the combustion products (flue gas) of solution gas and transferring it to a client unit where electricity is produced. The ultimate objective of the recovery system is the generation of electricity to inject enough air for the complete combustion of solution gas that is flared in order to reduce greenhouse gas emissions and smoke formation. The schematic diagram of the proposed system is shown in Figure 1.1.

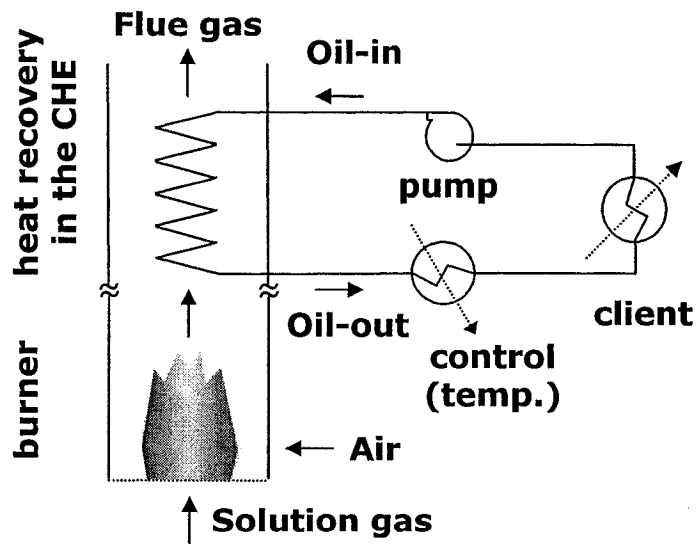

Figure 1.1 Components of the proposed heat recovery system for flue gas streams.

The thermal energy from the flue gas is recovered by a working fluid (e.g., heat transfer oil) in a Coil Heat Exchanger (CHE) placed in the incinerator stack. Heat is transferred to the boiler of a commercial Organic Rankine Cycle Engine (the client) where 7.52 kW of electricity is produced. The specified heat flow and the inlet and outlet oil temperatures from the client are the main operating specifications. A heat exchanger regulates the oil temperature at the client inlet to ensure the right load while a pump provides circulation. The client's thermal load is 69.6 kW and the specified inlet and outlet oil temperatures are 180°C and 123.4°C, respectively.

In order to estimate the feasibility of this system one would have to calculate the surface area for heat transfer between the flue gas and the oil stream. Variations in flue gas properties (temperature and flow rate) and an effective control strategy would have to be considered so as to meet client specifications (oil temperature and heat load) beyond design conditions.

The heat recovery system has been designed for an oil or bitumen site with an annual volume of solution gas flared or vented that is of the same order as the mean annual volume for all physical sites of 247 000 m^3/year (see §1.1). In 1999 there were 487 sites with monthly variations of less than 100% from the average volume that processed between 100 000 m^3/year and 316 200 m^3/year (Johnson et al., 2001). Apart from the steadiness of the solution gas source, other considerations before implementing this heat recovery system should be the use of the electricity produced and the possibility of servicing the burner, the control equipment and the ORCE itself. Hence flares in remote areas are ruled out for the moment in favour of larger oil or bitumen sites and gas plants.

1.4 Objectives and Scope

The primary objectives of this work are 1) to analyse the combustion reaction of solution gas in excess air in order to obtain the mass flow rate and a reasonable estimate of the temperature of the flue gas stream; 2) to design the CHE where the flue gas transfers

some of its heat to the oil. The information required includes the exchanger configuration, its surface area and materials of construction. The mathematical model should take into consideration the main processes of heat transfer present between the flue gas and the oil; 3) to utilize the mathematical model to carry out parametric studies of the design and performance problems for flue gas conditions different from those in the reference case. Specifically this includes the effect of mass flow rate and temperature of the flue gas on the size of the CHE and on the oil temperature leaving an existing CHE. Details about the burner, the control and client units are beyond the scope of this work.

2 Modelling Methodology

This chapter presents the theory and design approach employed to model the combustion reaction of solution gas in excess air (§2.1) and the heat transfer mechanisms in the Coil Heat Exchanger (§2.2). Finally, the mathematical solution of the steady state heat transfer model for both the design and performance scenarios of the heat exchanger is presented in §2.2.8.

2.1 Combustion Calculations

2.1.1 Material Balance

The objectives of the material balance are to calculate the amount of combustion air based on the nominal rate of solution gas and a fixed stoichiometric number (λ_A); secondly, to determine the composition and mass flow rate of the combustion products (flue gas).

In the reference case solution gas is modelled as a stream of pure methane gas (CH_4) that reacts with air in a burner at atmospheric pressure (see Figure 2.1). The nominal flow rate of methane is given and corresponds to the average annual volume of solution gas flared or vented at all physical batteries in Alberta (see §1.1). Combustion air is modelled as containing 21% oxygen (O_2) and 79% nitrogen (N_2) by volume. It is supplied 25% in excess of the stoichiometric amount (λ_A = 1.25). The combustion process is represented in Figure 2.1.

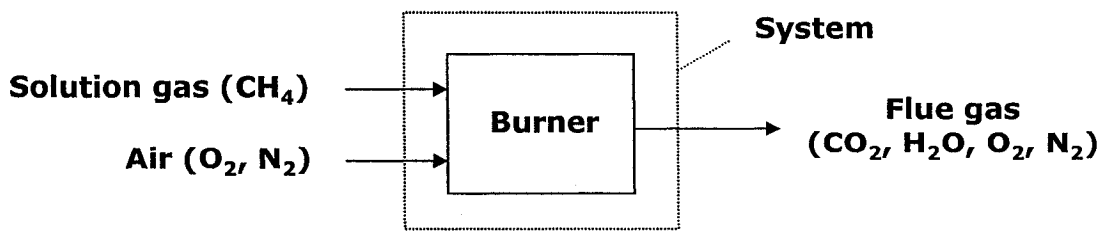

Figure 2.1 Feed and product streams in the solution gas burner.

The material balance to determine the amount of combustion air and the concentration of flue gas is based on the following assumptions: 1) steady state, 2) ideal gas behaviour, and 3) complete combustion of solution gas according to the reaction:

$$CH_4 + 2O_2 \rightarrow CO_2 + H_2O \qquad (2.1)$$

Volumes are reported at standard temperature and pressure (STP) for inlet and outlet streams ($T = 0^oC$ and $P = 1$ atm). The amount of combustion air is calculated based on the stoichiometric amount of oxygen required to react with methane according to Eq. (2.1) and the air number provided. Combustion products (CO_2 and H_2O) are computed from Eq. (2.1) and the nominal flow rate of methane. An example of these calculations can be found in Himmelblau and Riggs (2004). The mass flow rate of the flue gas is the sum of the nominal flow rate of methane and the amount of combustion air.

2.1.2 Theoretical Flame Temperature

Once the composition of the flue gas is known, the temperature of the flame may be calculated under certain assumptions. This temperature will be influenced by the quantity of inert compounds present and thus it will depend on λ_A. Heat losses due to radiation and convection along the stack section between the burner and the Coil Heat Exchanger may reduce significantly the temperature of the flue gas from the flame temperature.

For an adiabatic process and when there is no work or other effects present (e.g., electrical effects, ionization, free radical formation), the temperature of the combustion reaction reaches a maximum, known as the theoretical flame temperature (TFT). It can be calculated by solving an energy balance equation at steady state where the terms for the heat and work exchanged with the environment are set to zero (Himmelblau and Riggs, 2004). In our calculations, heat capacities of real gases at low pressures were approximated by those of ideal gases (Smith et al., 1996).

Flue gas composition and TFT analysis of gaseous mixtures with more than one component and for different levels of excess air can be carried out in a spreadsheet that was developed for this purpose (see Appendix A). The spreadsheet has been written in a general way to include mixtures of a large number of gases in addition to methane. However, pure methane alone was considered for the design of the heat exchanger.

2.2 Heat Exchanger Design

The heart of the heat recovery system is the Coil Heat Exchanger (CHE) placed on the upper part of the stack. It is there that the flue gas transfers part of its thermal energy to the oil stream. This section presents the design equations for the CHE surface area based on the solution of a series of steady state energy balances. It discusses an approach to include convection, radiation and conduction heat transfer processes occurring in the coil section of the stack. Heat losses are foreseen in the calculations and will be minimized by proper insulation around the stack. The main objective is to present a methodology to estimate the surface area of the coil heat exchanger given the client specifications and flue gas available (design scenario). Once the surface area has been fixed, a similar methodology is presented that will allow for the calculation of the oil temperature at the CHE exit when the temperature and flow rate of the flue gas stream change (performance scenario). All these calculations depend on algebraic equations for the thermo-physical properties of the flue gas and oil streams as well as the actual geometry of the system (e.g., coiled tube diameter) and the materials of construction. Geometry and materials issues are addressed in more detail in §§3.2 and 3.3.

2.2.1 Characterizing the Oil and Flue Gas Streams

The first step in designing the CHE is to define the mass flow rate and inlet and outlet temperatures of the oil and flue gas streams. The system specifications (see §1.3) had fixed the rate of heat flow required by the client (Q_{cl}) and the oil temperatures at the inlet (T-Oil-4) and outlet (T-Oil-5) of the client unit as shown in Figure 2.2.

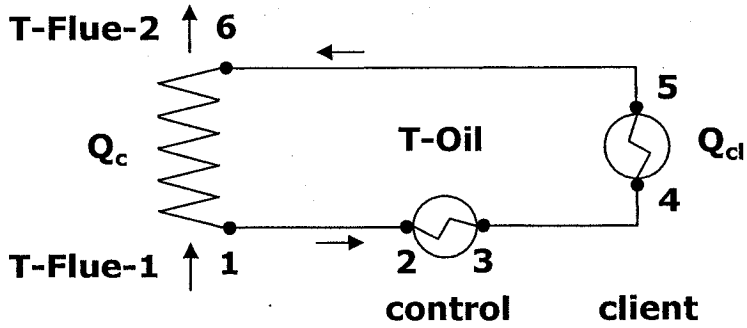

Figure 2.2 Temperatures of interest for the flue gas and oil streams in the heat recovery system.

Through a simple energy balance around the client unit, the mass flow rate of oil may be obtained:

$$M_{Oil} = \frac{-Q_{cl}}{\int_{T-Oil-4}^{T-Oil-5} C_{P,oil}\, dT} \tag{2.2}$$

Assuming no thermal losses along the oil loop, the oil temperature at the inlet of the CHE (T-Oil-6) is equal to T-Oil-5 and the oil temperature at the coil outlet (T-Oil-1) is equal to T-Oil-4.

The initial information about the flue gas stream comprised its mass flow rate and the temperature at the point of contact with the CHE (T-Flue-1). The mass flow rate of flue gas is derived in §2.1.1. It is necessary to assume T-Flue-1 since details of the burner are unknown. The outlet flue gas temperature T-Flue-2 depends on the heat transferred to the oil stream and any heat losses to the environment. Heat losses may be minimised by a proper insulation strategy.

2.2.2 Elements of the Analysis: Control Volume Definition and Temperature Profile

The mathematical solution of the heat transfer model for the CHE consists of dividing the stack and heat exchanger into cylindrical control volumes (CV). The length of coiled tube in each section (Δx) was the basis for the definition of a CV. In this case, the height of a CV (Δy) is given by

$$\Delta y = b\, \Delta x / l_{turn} \tag{2.3}$$

where b is equal to the coil pitch and l_{turn} is the length of one full turn of the coiled tube (For the majority of simulations, Δx was set equal to l_{turn} and Δy was set equal to b).

The temperature profile of one CV (see Figure 2.3) identifies all the terms used in the energy balance equations. The stack (D_s) and coiled tube (D_c) diameters follow the same notation of subscript numbers as those of the temperature terms (e.g., T_{c2} refers to the temperature on the outside of the coiled tube and D_{c2} refers to the external diameter of the coiled tube).

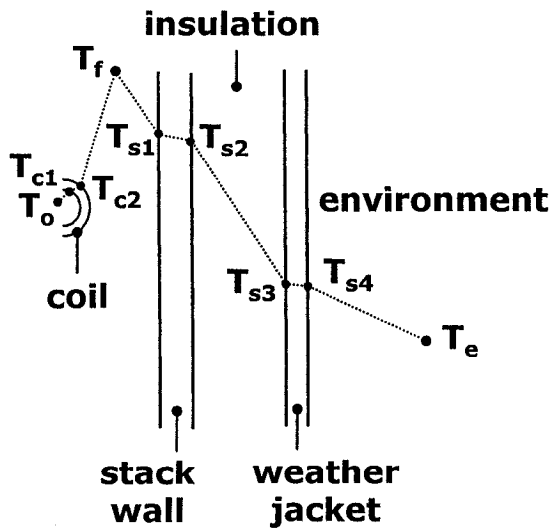

Figure 2.3 Temperature profile in a CV of the CHE.

2.2.3 Modes of Heat Transfer and Thermal Circuit

The flue gas exchanges heat with the oil and the environment. Conduction, convection and radiation mechanisms are all present and may be modelled by making some simplifying assumptions. These mechanisms can be grouped as follows:

- Transfer between the flue gas and the coiled tube: convection, radiation
- Transfer between the flue gas and the stack: convection
- Transfer between the stack and the environment: conduction, convection
- Transfer between the coiled tube and the oil: conduction, convection

A useful tool to visualize the heat transfer mechanisms is the thermal circuit that relates heat flow [W] and temperature differences [°C] through the concept of the resistance to heat transfer [°C/W] (see Figure 2.4). This resistance is the inverse of the product of the heat transfer coefficient [W/m^2°C] and the appropriate area for heat transfer, and is specific to each of the modes of heat transfer. An explanation of each term in the thermal circuit follows.

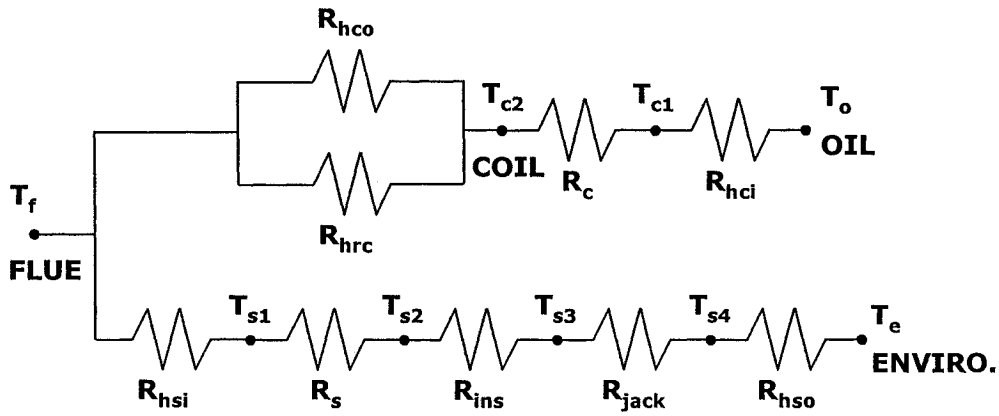

Figure 2.4 Thermal circuit between the flue gas, oil and the environment.

Heat losses to the environment play an important role in the modelling strategy. In order to model the heat flow leaving the CHE, the temperature of the environment had to

appear in the analysis. The presence of three temperature nodes (flue gas, oil and environment) precluded the definition of an overall heat transfer coefficient between the flue gas and the oil temperatures and therefore discouraged the use of the Log Mean Temperature Difference (LMTD) or Number of Transfer Units (NTU) methods of heat exchanger design.

Resistance terms between the flue gas and the coiled tube: convection and radiation

In every CV heat is transferred from the flue gas to the external surface of the coiled tube by convection and by radiation. Hence both mechanisms occur in parallel as shown in Figure 2.5 where the convection resistance is R_{hco}, the radiation resistance is R_{hrc} and the combined resistance is R_{fc} (from the flue gas to the coiled tube).

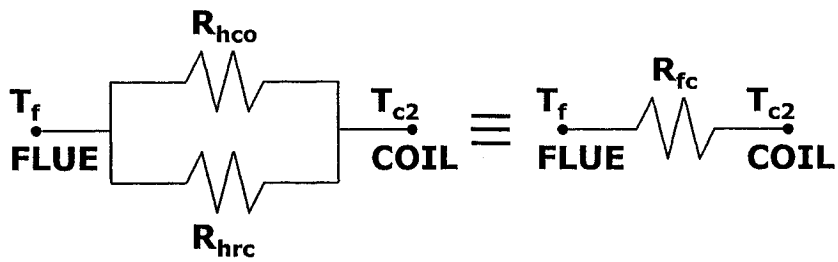

Figure 2.5 Convection and radiation resistances between the flue gas and the coiled tube.

Both resistances are based on the external surface area of the coiled tube in the CV, which is equal to $\pi D_{c2}\Delta x$. The convection (h_{co}) and radiation (h_{rc}) heat transfer coefficients also appear in the definition of the resistance terms:

$$\text{Convection}: \quad R_{hco} = \frac{1}{\pi D_{c2} \Delta x h_{co}} \tag{2.4}$$

$$\text{Radiation}: \quad R_{hrc} = \frac{1}{\pi D_{c2} \Delta x h_{rc}} \tag{2.5}$$

Combined resistance from the flue gas to the coiled tube:

$$R_{fc} = \frac{1}{\pi D_{c2} \Delta x (h_{co} + h_{rc})} \tag{2.6}$$

It should be noted that R_{fc}, unlike the convective counterpart, is not a simple resistance but instead includes nonlinear effects associated with radiative heat transfer. As discussed later (see §2.2.5), the radiation term includes the stack's radiosity to the coiled tube through a radiating medium (due to the water vapour and carbon dioxide in the flue gas). However since the net exchange of heat by radiation was assumed to be between the flue gas and the coiled tube, the appropriate driving force for this circuit representation using R_{hrc} is $(T_f - T_{c2})$.

Resistance term between the flue gas and the stack: convection

For the flue gas in the gap between the coiled tube and the stack, the main heat transfer process will be convection since the net effect of radiation on the wall of the CV was assumed to be zero (see §2.2.5). Hence the overall resistance between the flue gas and the stack (R_{fs}) is the same as the convection resistance (R_{hsi}) as shown in Figure 2.6.

Figure 2.6 Convection resistance between the flue gas and the stack.

The area for heat transfer is the internal surface area of the stack in the CV, which is equal to $\pi D_{s1} \Delta y$. If expressed in terms of Δx (the basis for the definition of the CV), the stack surface area will be $\pi D_{s1} b \Delta x / l_{turn}$. The heat transfer coefficient due to internal convection of the flue gas in the stack is h_{si}. The resistance term becomes:

$$\text{Convection:} \quad R_{fs} = R_{hsi} = \frac{l_{turn}}{\pi D_{s1} b \Delta x h_{si}} \tag{2.7}$$

Resistance terms between the stack and the environment: conduction and convection

Any heat flow that reaches the inner stack surface is considered a heat loss from the CHE. In order to minimise this loss, insulation is added to the outer side of the stack. Heat is transferred by conduction through the stack and the insulation system (insulating material plus weather jacket). Once outside, heat will be dissipated by external convection of the air surrounding the insulated stack. All these processes happen in series (see Figure 2.7) and their resistance terms may be combined into one (R_{stack}).

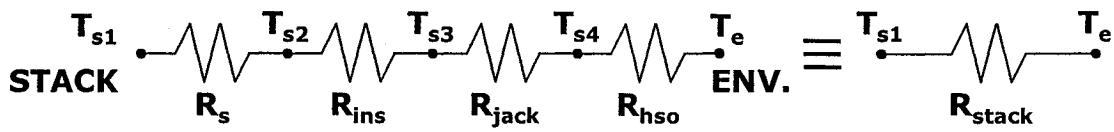

Figure 2.7 Conduction and convection resistances between the stack and the environment.

The four resistance terms are based on the height of CV (Δy), which can be expressed in terms of the length of coiled tube in the CV as $b\Delta x/l_{turn}$. Conduction resistances (R_s, R_{ins} and R_{jack}) across cylindrical shells are described by the inner and outer diameters of each shell and the thermal conductivity of the material. Only one-dimensional conduction is considered (i.e., no edge or curvature effects). The basis of the convection resistance is the outer surface area of the stack-plus-insulation system ($\pi D_{s4} b\Delta x/l_{turn}$). The value of the external heat transfer coefficient h_{so} was fixed *a priori* to simulate windy (60 W/m^2 °C) or calm (10 W/m^2 °C) conditions. The combined resistance term R_{stack} neglects the contact resistance between the stack and the insulation and between the insulation and the weather jacket. In the equations that follow, D_{s1} through D_{s4} are the diameters from the interior of the stack (D_{s1}) to the exterior surface of the insulation system (D_{s4}).

$$\text{Stack wall}: \quad R_s = \frac{l_{turn} \ln(D_{s2}/D_{s1})}{2\pi \lambda_s b \Delta x} \tag{2.8}$$

$$\text{Insulation}: \quad R_{ins} = \frac{l_{turn} \ln(D_{s3}/D_{s2})}{2\pi \lambda_{ins} b \Delta x} \tag{2.9}$$

$$\text{Weather jacket}: \quad R_{jack} = \frac{l_{turn} \ln(D_{s4}/D_{s3})}{2\pi \lambda_{jack} b \Delta x} \tag{2.10}$$

$$\text{External convection}: \quad R_{hso} = \frac{l_{turn}}{\pi D_{s4} b \Delta x h_{so}} \tag{2.11}$$

Combined resistance between the stack and the environment:

$$R_{stack} = \frac{l_{turn}}{2\pi b \Delta x}\left[\frac{\ln(D_{s2}/D_{s1})}{\lambda_s} + \frac{\ln(D_{s3}/D_{s2})}{\lambda_{ins}} + \frac{\ln(D_{s4}/D_{s3})}{\lambda_{jack}}\right] + \frac{l_{turn}}{\pi D_{s4} b \Delta x h_{so}} \tag{2.12}$$

Resistance terms between the coiled tube and the oil: conduction and convection

For the heat to reach the oil from the outer surface of the coiled tube it has to travel through tube itself by conduction and then through the flow of oil by convection. Figure 2.8 illustrates thermal circuit for these two processes in series. (Fouling of the outer surface of the coiled tube is not considered for the sake of simplicity).

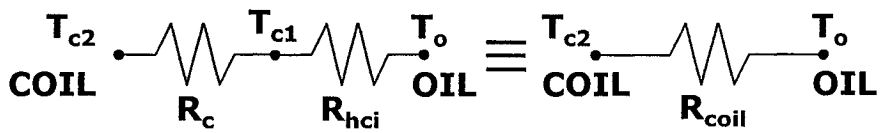

Figure 2.8 Conduction and convection resistances between the coiled tube and the oil.

Both resistance terms are based on the length of coiled tube in the CV (Δx). The one-dimensional conduction resistance R_c across the coiled tube depends on the tube's inner (D_{ci})

and outer (D_{c2}) diameters and the thermal conductivity of the material. The basis of the convection resistance is the inner surface area of the coiled tube ($\pi D_{c1}\Delta x$) and the convective heat transfer coefficient h_{ci}.

$$\text{Coiled tube}: \quad R_c = \frac{\ln(D_{c2}/D_{c1})}{2\pi\lambda_c \Delta x} \tag{2.13}$$

$$\text{Internal convection}: \quad R_{hci} = \frac{1}{\pi D_{c1} \Delta x h_{ci}} \tag{2.14}$$

Combined resistance between the coiled tube and the oil:

$$R_{coil} = \frac{1}{\pi D_{c1} \Delta x h_{ci}} + \frac{\ln(D_{c2}/D_{c1})}{2\pi\lambda_c \Delta x} \tag{2.15}$$

Overall thermal circuit (compact configuration)

Having defined several combined resistance terms, the thermal circuit of Figure 2.4 may be presented more compactly as follows:

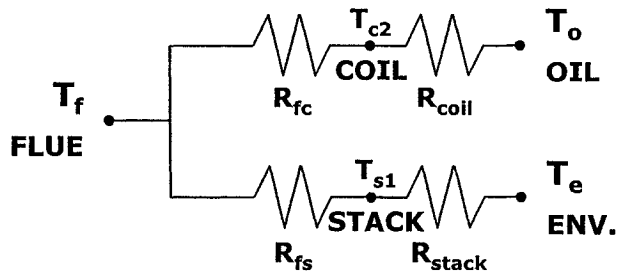

Figure 2.9 Overall thermal circuit between the flue gas, oil and the environment (compact configuration).

Note that R_{fc} does not depend directly on T_{s1} since the walls of the CV are assumed adiabatic and T_{s1} will not appear in the radiation equations, e.g., Eq. (2.37) or Eq. (2.38). In contrast all the terms that define the radiation heat flux at the coiled tube surface in Eq.

(2.34) depend on T_{c2}. Nonetheless, R_{fc} depends indirectly on T_{s1} inasmuch as it affects the transmissivity of the flue gas (see §2.2.5).

2.2.4 Convection and Conduction Processes

In convection processes, heat is transferred due to the relative motion of two bodies. Heat transfer by conduction occurs within a body itself. Both are driven by a temperature difference, either between two bodies in relative motion (convection) or between two sides of the same body (conduction). In order to model convection and conduction heat transfer processes three elements are necessary: thermo-physical properties of the bodies, the temperature at which to evaluate the properties and, in the case of convection, the appropriate correlations for the Nusselt number.

Convection appears both as an internal and an external process. Internal convection applies to the oil in the coiled tube (as opposed to the flue gas flowing over the coiled tube). It also applies to the flue gas in the stack (compared to the air in the environment surrounding the stack). For internal convection processes, the Nusselt number may be affected by entrance effects and variable property effects as discussed below (Mills, 1999). External convection defines the transfer of heat of the flue gas flowing over the coiled tube and of the air surrounding the stack.

The Nusselt number correlations for internal and external convection are expressed in terms of dimensionless numbers such as the Reynolds and the Prandtl numbers. The Reynolds number of a stream flowing over or inside a cylinder of diameter D is defined as

$$\mathrm{Re}_D = \frac{uD}{\nu} \tag{2.16}$$

where u is the stream's average bulk velocity in m/s and ν is its kinematic viscosity in m/s^2. The inner diameter of the cylinder is used for the Reynolds number of an internal flow and

the outer diameter for external flows. All the Reynolds numbers in this work were turbulent indicating forced convection regime. Natural convection processes were thus neglected. The average bulk velocity of a stream in a duct may be calculated from the mass flow rate, density and cross-section of the duct:

$$u = \frac{4M}{\rho \pi D_{inner}^2} \tag{2.17}$$

The Prandtl number indicates the relative weight of momentum transfer to heat transfer processes in a stream. It is defined as

$$\mathrm{Pr} = \frac{\eta C_P}{\lambda} \tag{2.18}$$

where η is dynamic viscosity in kg/m·s, C_P is heat capacity in J/kg°C and λ is thermal conductivity in W/m°C.

Finally the heat transfer coefficient (h) is related to the Nusselt number through the definition of the Nusselt number:

$$Nu = \frac{hD}{\lambda} \tag{2.19}$$

where D is the characteristic length on which the Reynolds number is based.

Internal convection of the oil in the coiled tube

The oil stream in the coiled tube absorbs the heat from the flue gas by forced internal convection, which is characterized by the heat transfer coefficient h_{ci}. The peculiarity of this flow is that it occurs in a coiled duct, which increases the heat transfer coefficient over the case of a straight circular duct. This effect is discussed below. The thermo-physical properties of the oil are evaluated at the average bulk temperature of the oil in the CV, which

is assumed to be the oil temperature leaving the CV (see the Well-Mixed assumption in §2.2.6).

From these properties, the Reynolds and Prandtl numbers can be calculated with the internal diameter of the coiled tube (D_{cl}) as the characteristic length. The Nusselt number is determined by the Gnielinski correlation for flow inside a cylinder. This correlation agrees with most available experimental data within 20% (Mills, 1999) and is applicable for flows where $Pr > 0.5$ and $3000 < Re_D < 1\,000\,000$.

$$Nu_D = \frac{(f/8)(\mathrm{Re}_D - 1000)\,\mathrm{Pr}}{1 + 12.7(f/8)^{1/2}(\mathrm{Pr}^{2/3} - 1)} \tag{2.20}$$

where f is the friction factor in the coiled tube described by the Petukhov formula for smooth inner walls and for $Re_D < 5\,000\,000$ (Mills, 1999):

$$f = (0.790\ln(\mathrm{Re}_D) - 1.64)^{-2} \tag{2.21}$$

There are two corrections that need to be applied to this Nusselt number. The first one is for variable property effects that account for the different temperature at the wall of the coiled tube (T_{cl}) compared to the average bulk temperature of the oil (T_o). Since the temperature gradient between the wall and the oil occurs across a very thin layer near the wall, this correction is meant to adjust the Nusselt number to represent better the properties of the oil in that layer. The correction factor for a liquid under a *heating* wall condition is the ratio of the liquid's dynamic viscosity at those two temperatures (Mills, 1999). It is expected that this correction factor will be around 5% and thus will not be a significant factor:

$$Nu_o = Nu_b \left(\frac{\eta_{Tcl}}{\eta_{To}} \right)^{-0.11} \tag{2.22}$$

The second correction is due to the coiled duct itself. As the oil flows within a curved tube it experiences a centrifugal force and an axial pressure gradient. The centrifugal force generates a secondary flow over the normal axial flow which increases the main flow's (axial) velocity near the tube's outer wall (relative to the main flow) and decreases the axial velocity near the tube inner wall. The net result is higher heat transfer coefficients and friction factors than in straight tubes. The Schmidt correlation provides the correction factor for the Nusselt number (Shah and Joshi, 1987):

$$\frac{Nu_{ci}}{Nu_o} = 1 + 3.6\left(1 - \frac{D_{cl}}{2R_c}\right)\left(\frac{D_{cl}}{2R_c}\right)^{0.8} = 1.67 \qquad (2.23)$$

where R_c is the radius of curvature of the coiled tube. Although the value of 1.67 is significant, its effect will not be so since the smaller (and therefore controlling) heat transfer coefficient will be on the gas side and not on the oil side.

For turbulent flows in long tubes and Pr >> 1, entrance effects can be neglected. The value of the heat transfer coefficient h_{ci} is then obtained from Eq. (2.19).

Internal convection of the flue gas in the stack

In the calculation of the thermal losses to the environment, it is necessary to estimate the heat transfer coefficient of the flue gas in the gap between the coiled tube and the inside of the stack (h_{si}). The properties of the flue gas are evaluated at the average bulk temperature of the gas in the CV that is assumed to be the gas temperature leaving the CV (see §2.2.6).

From the thermo-physical properties of the flue gas, the Reynolds and Prandtl numbers can be calculated. The Reynolds and Nusselt numbers should be based on the internal diameter of the stack (D_{sl}). The Nusselt number is determined by the Gnielinski correlation for flow inside a cylinder. Its boundaries of applicability are flows where Pr > 0.5 and $3000 < Re_D < 1\,000\,000$.

$$Nu_D = \frac{(f/8)(\mathrm{Re}_D - 1000)\,\mathrm{Pr}}{1 + 12.7(f/8)^{1/2}(\mathrm{Pr}^{2/3} - 1)} \tag{2.24}$$

where f is the friction factor in the stack. Assuming a smooth inner wall, the Petukhov formula can be used to estimate the friction factor for $\mathrm{Re}_D < 5\,000\,000$ (Mills, 1999):

$$f = (0.790\ln(\mathrm{Re}_D) - 1.64)^{-2} \tag{2.25}$$

Using the average bulk velocity of the gas in the empty stack (see Eq. (2.17)) to represent the gas velocity in the gap between the coiled tube and the stack is a crude approximation. The presence of the coiled tube near the stack wall will result in a thick boundary layer at the wall so that the gas flow in the gap will be slower than in the middle of the CHE. This approximation will overestimate the heat losses to the environment and the temperature on the inner side of the stack. In turn this overestimation of the stack temperature will yield a more conservative recommendation for the maximum flow rate of flue gas through the system that respects the maximum service temperature of the construction material (see §3.4.1).

If the flow of flue gas is turbulent and its Prandtl number close to unity, entrance effects will increase the Nusselt number above its fully developed value given by Eq. (2.24). Assuming the geometry of a long calming section and for a CHE height equal to five times the stack's inner diameter ($H/D_{sI} = 5$), the Nusselt number is 1.3 times larger than the fully developed value (by interpolation from Table 4.4 in Mills, 1999). This value was kept constant throughout the parametric studies, reinforcing the logic behind the overestimation of the stack temperature mentioned above.

Variable property effects may be neglected if the flow is turbulent and the flue gas is being cooled (i.e., *cooling* wall condition). In this case the exponent of the correction factor for $\mathrm{Nu_D}$ is zero (Mills, 1999). For a gas, the correction factor is the ratio of the gas temperature at the wall to the bulk gas temperature.

The heat transfer coefficient of the flue gas inside the stack (h_{si}) is expressed with respect to the internal diameter of the stack (D_{s1}) and can be derived from the definition of the Nusselt number:

$$h_{si} = 1.3 \frac{Nu_D \lambda_{Flue}}{D_{s1}} \tag{2.26}$$

where the value of 1.3 is the correction factor for entrance effects.

External convection of the flue gas over the coiled tube

This is one of the two parallel mechanisms by which the flue gas transfers heat to the outer surface of the coiled tube. If radiation were not present, the argument for the external convection heat transfer coefficient (h_{co}) being the rate-limiting process would be even stronger since it will be significantly smaller than the internal heat transfer coefficient of the oil in the coiled tube (h_{ci}).

In order to determine the external heat transfer coefficient, the thermo-physical properties of the flue gas are evaluated at the mean film temperature, which is the average of the flue gas bulk temperature in the CV and the temperature on the outside of the coiled tube (T_{c2}). As in the case of the oil, the average bulk temperature of the flue gas is assumed to be equal to the gas temperature at the exit of the CV (see §2.2.6).

From the thermo-physical properties of the flue gas, the Reynolds and Prandtl numbers can be calculated. The Reynolds number should be based on the external diameter of the coil tube (D_{c2}). For a Reynolds number less than 10 000, the appropriate Churchill and Bernstein correlation can be used to estimate the Nusselt number (Mills, 1999). Since these correlations apply to forced flow over a cylinder, it is necessary to assume that the section of the coiled tube in the CV could be approximated by a straight cylinder.

$$Nu_D = 0.3 + \frac{0.62\,\mathrm{Re}_D^{1/2}\,\mathrm{Pr}^{1/3}}{\left(1+\left(\frac{0.4}{\mathrm{Pr}}\right)^{2/3}\right)^{1/4}} \tag{2.27}$$

As in the case of h_{si}, the Reynolds number to describe the flow of flue gas over the coiled tube is based on the free stream velocity of gas in the empty stack. This may be justified here as a way to compensate for the flow deficiency of flue gas in the gap between the coiled tube and the stack, and the velocity increase in the middle of the CHE due to the reduction in space for the flue gas to flow caused by the coiled tube. The presence of the coiled tube causes an effective thickening of the wall boundary layer for the flue gas.

No variable property effects corrections are needed since the properties for the Churchill and Bernstein correlations are evaluated at the mean film temperature. The heat transfer coefficient of the flue gas over the coiled tube (h_{co}) depends on the external diameter of the coil tube (D_{c2}) and can be derived from the definition of the Nusselt number in Eq. (2.19). Compared to the internal heat transfer coefficient, the external heat transfer coefficients by convection and radiation are expected to be smaller and thus to control the flow of heat to the oil.

External convection of the air around the stack

The value of the external heat transfer coefficient h_{so} was fixed *a priori* to simulate windy (60 W/m^2°C) or calm (10 W/m^2°C) conditions. For comparison, a typical value of h_{co} (convection of the flue gas over the coiled tube) was 45 W/m^2°C.

Conduction resistance to heat transfer in cylindrical coordinates

Conduction heat transfer is not normally characterized by the concept of the heat transfer coefficient as in the case of convective processes. Instead the resistance to heat transfer due to conduction is used. In the case of one-dimensional conduction, this resistance is a function of the geometry of the material and its thermal conductivity. The thermal conductivity should be evaluated at the mean temperature of the material, which implies knowing the temperature profile across the system (coiled tube and the insulated stack) and

having the appropriate temperature correlations of the thermal conductivity for each material. The expressions for the resistance due to conduction appear in §2.2.3.

2.2.5 Radiation Processes

The two parallel modes of heat transfer between the flue gas and the outer surface of the coiled tube are external convection of the flue gas and radiation. The sources of radiation are the stack and the flue gas itself. (Direct radiation from the flame is not considered since the CHE is assumed to be at the top of the flare stack, away from the flame; see Figure 1.1). The stack's temperature is always higher than the temperature of the coiled tube since the coiled tube is being cooled down by the flow of oil. The flue gas absorbs and emits radiation in finite bands of the spectrum due to the presence of non-symmetrical molecules like water vapour and carbon dioxide. The flue gas will also attenuate the radiation from the stack to the coiled tube. The effect of aerosols (liquid droplets, dust and soot particles) that also emit and absorb radiation has been neglected.

The radiation analysis is based on the exchange equations for radiation between a gas enclosed in grey solid surfaces. The general equations are found in Hottel and Sarofim (1967). After applying these equations to the CV to derive the expression of the radiation heat transfer coefficient (§2.2.3), we will look at the evaluation of flue gas properties like emissivity, absorptivity and transmissivity.

For the purposes of radiation transfer, the CV contains one full turn of the coiled tube. The effect of the length of the coiled tube in the CV on the overall solution is presented in §3.4.3. The wall of the CV (side, top and bottom) is assumed adiabatic. This may be justified by the fact that the side wall is insulated and the application of the Long Furnace assumption to the top and bottom surfaces of the CV. The Long Furnace assumption considers only transfer processes in the transverse direction to the main flow (i.e., at 90^{o} of the main flow). The assumption states that any heat entering a CV from a previous CV is similar in magnitude to the heat flowing from this CV to the next one. Thus the net effect of that transfer mechanism on the CV is negligible. This simplification is reasonable when the

flue gas temperature (or the variable that provides the driving force for the transfer mechanism) does not change rapidly from one CV to the next (see Figure 3.7). In this work this assumption applies to radiation and conduction transfer between adjacent CV. The temperature of the wall of the CV (T_{s1}), that of the coiled tube (T_{c2}) and of the flue gas (T_f) are also assumed to be constant in each CV (see Figure 2.10).

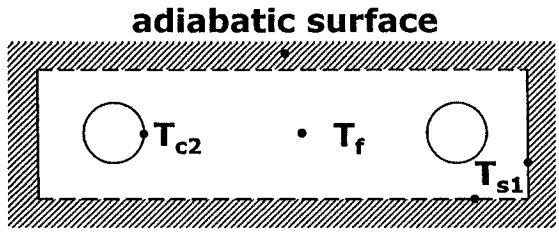

Figure 2.10 Assumed geometry of CV for the estimation of the radiation resistance.

At any grey surface (wall or coiled tube), the outgoing radiation J_i (or "radiosity") includes the emission from the surface (by virtue of its temperature and emissivity) and any portion of the incoming radiation that is reflected (only black surfaces absorb all incoming radiation). The incoming radiation G_i (or "irradiation") combines the radiosity of all the other surfaces attenuated by the transmissivity of the gas and the radiation from the flue gas itself. The relative position of the surfaces is described by the view factor between them. It was assumed that the coiled tube was small compared to the volume of the CV and that therefore all it "sees" are the walls of the CV. Thus the view factor F_{cs} that describes the fraction of the coil's environment that is taken up by the stack (or wall), was one (i.e., 100%) and F_{cc} was equal to zero since the coil's field of vision was ideally occupied by the stack. It is useful to know that F_{cs} is associated with the radiation from the stack to the coil and F_{sc} describes the exchange from the coil to the stack. View factor algebra relates surface area and view factors as follows

$$A_s F_{sc} = A_c F_{cs} \tag{2.28}$$

and thus

$$F_{sc} = \frac{A_c}{A_s} F_{cs} = \frac{D_{c2}\Delta x}{\frac{D_{s1}^2}{2} + D_{s1} \cdot \frac{b\,\Delta x}{l_{turn}}} \tag{2.29}$$

where $F_{cs} = 1$. The view factor F_{ss} can be calculated from the relationship

$$F_{ss} + F_{sc} = 1 \tag{2.30}$$

The coiled tube is a grey surface with emissivity $\varepsilon_c = 0.5$ which applies to stainless steel up to 900°C (Mori et al., 1980) and assumes that there is little soot in the flue gas. This is consistent with the ultimate goal of the heat recovery system of generating electricity to inject enough air in order to achieve complete combustion of solution gas and thus reduce smoke (i.e., soot) formation.

All the elements are now available to write the radiation exchange equations for the CV under the stated assumptions. The radiation heat transfer coefficient in Eq. (2.5) will be derived not from correlations (as in the case of convection) but from the definition of the coefficient itself as the ratio of the net heat gain by radiation at the coiled tube surface and the appropriate temperature difference.

Two surface energy balances are required, one on the outside of the coiled tube and another on the wall of the CV. At the coiled tube surface the incoming irradiation G_c is comprised by 1) the radiosity from the wall to the coil attenuated by the transmissivity of the flue gas ($F_{cs}\tau_{f,Ts1}J_s$) and 2) the radiation from the flue gas itself ($F_{cs}\,\varepsilon_{f,Tf}\,\sigma T_f^4$) emitted at T_f. There is no self irradiation from the coiled tube since $F_{cc} = 0$. The net heat loss at the coiled tube surface q_{rc} [W/m^2] is obtained by subtracting G_c from the outgoing radiation from the coil J_c:

$$q_{rc} = J_c - G_c = J_c - (F_{cc}\tau_{f,Tc2}J_c + F_{cc}\varepsilon_{f,Tf}E_{b,f}) - (F_{cs}\tau_{f,Ts1}J_s + F_{cs}\varepsilon_{f,Tf}E_{b,f}) \tag{2.31}$$

where subscripts T_{s1} and T_{c2} on the transmissivity terms indicate that the radiation transmitted through the flue gas at T_f was emitted originally at the wall temperature T_{s1} or the coiled tube temperature T_{c2}; ε_f is the emissivity of the gas and $E_{b,f}$ is the emissive power of a hypothetical black body at the same temperature as the gas (= σT_f^4, W/m^2). Note that Eq. (2.31) further simplifies since $F_{cc} = 0$ and $F_{cs} = 1$.

Another expression for q_{rc} in terms of the emissivity of the coil surface can be obtained from the definition of the radiosity leaving the coil, which includes emission and reflection terms:

$$J_c = \varepsilon_c E_{b,c} + \rho_c G_c \tag{2.32}$$

where $E_{b,c}$ is the blackbody emissive power of the coil surface (= σT_{c2}^4, W/m^2) and ρ_c is the reflectivity of the coiled tube. For an opaque surface, ρ_c is equal to one minus the absorptivity of the surface ($1 - \alpha_c$). Solving for the irradiation arriving at the coil

$$G_c = \frac{J_c - \varepsilon_c E_{b,c}}{1 - \alpha_c} = \frac{J_c - \varepsilon_c E_{b,c}}{1 - \varepsilon_c} \tag{2.33}$$

where the absorptivity of a grey body has the same value as its emissivity (ε_c). Substituting this expression in the definition of the net heat loss as J_c minus G_c yields

$$q_{rc} = \frac{\varepsilon_c}{1 - \varepsilon_c}(E_{b,c} - J_c) \tag{2.34}$$

Finally, combining Eq. (2.31) and Eq. (2.34) we can solve for the radiosity leaving the coil:

$$J_c = \varepsilon_c \sigma T_{c2}^4 + (1 - \varepsilon_c)(\tau_{f,Ts1} J_s + \varepsilon_{f,Tf} \sigma T_f^4) \tag{2.35}$$

For the second surface balance on the wall of the CV a similar expression to Eq. (2.31) can be written

$$q_{rs} = J_s - G_s = J_s - (F_{ss}\tau_{f,Ts1}J_s + F_{ss}\varepsilon_{f,Tf}E_{b,f}) - (F_{sc}\tau_{f,Tc2}J_c + F_{sc}\varepsilon_{f,Tf}E_{b,f}) \quad (2.36)$$

This expression is useful since it relates J_s to J_c and it is equal to zero since the walls of the CV were assumed adiabatic in the context of radiation transfer ($q_{rs} = 0$). The solution procedure is to solve Eq. (2.35) and Eq. (2.36) simultaneously for J_c and J_s. Then from Eq. (2.34) we may calculate q_{rc}, which should be negative since it is defined as a heat loss from the coil and the coil actually receives heat, i.e., $G_c > J_c$. The final equations are

$$J_s = \frac{\varepsilon_{f,Tf}\sigma T_f^{\,4} + F_{sc}\tau_{f,Tc2}\cdot\left[\varepsilon_c\sigma T_{c2}^{\,4} + (1-\varepsilon_c)\varepsilon_{f,Tf}\sigma T_f^{\,4}\right]}{1 - F_{ss}\tau_{f,Ts1} - F_{sc}\tau_{f,Tc2}(1-\varepsilon_c)\tau_{f,Ts1}} \quad (2.37)$$

$$J_c = \varepsilon_c\sigma T_{c2}^{\,4} + (1-\varepsilon_c)\cdot(\tau_{f,Ts1}J_s + \varepsilon_{f,Tf}\sigma T_f^{\,4}) \quad (2.38)$$

It is interesting to note two terms in Eq. (2.38): $\tau_{f,Ts1}J_s$, the radiation arriving at the coil from the wall and $\varepsilon_{f,Tf}\sigma T_f^4$, the radiation from the flue gas. Their relative magnitude will be discussed in §3.4.2.

At this point the only unknowns in Eq. (2.37) and Eq. (2.38) are the radiation properties of the flue gas (emissivity ε, transmissivity τ). It was stated earlier that a gas containing non-symmetrical molecules will absorb and emit radiation in finite bands. The absorption bands of gases are actually arrays of lines at discrete wavelengths. In order to estimate the total gas properties we follow the equations from the averaging process referred to in Perry and Green (1997). In that reference, equations are listed for gases with water vapour only or carbon dioxide only, and for gases with mixtures of different compositions of the two species. We chose the latter based on the composition of the flue gas from the reference case (pure methane burning in 25% excess air) with $p_{H2O} = 0.155$ atm and $p_{CO2} = 0.0775$ atm. More accurate methods based on band models were not explored. Gas emissivity

and transmissivity depend on the flue gas temperature (and on the surface temperature in the case of the transmissivity). These properties are also affected by the partial pressure of water vapour and carbon dioxide, and the average mean beam length in the CV. Partial pressures are obtained from the mole fractions of water vapour and carbon dioxide in the flue gas (§3.1). The average beam length concept arises from the fact that gas radiation is a volumetric phenomenon and not a surface one as in the case of solid body radiation. The mean beam length serves to characterize the volume of gas in the CV. Perry and Green (1997) suggest that for an arbitrary volume of gas in an enclosure of surface area A, a reasonable estimate of the mean beam length (L_m) is

$$L_m = 3.5\frac{V_{gas\ in\ CV}}{A_{CV}} = 3.5\frac{V_{CV} - V_{coil}}{A_{CV}} \tag{2.39}$$

where the volume and area terms may be expressed in terms of already defined variables:

$$L_m = 3.5\frac{\left(\frac{\pi D_{s1}^2}{4}\frac{b\Delta x}{l_{turn}} - \frac{\pi D_{c2}^2 \Delta x}{4}\right)}{\frac{\pi D_{s1}^2}{2} + \frac{\pi D_{s1} b\Delta x}{l_{turn}}} \tag{2.40}$$

Perry and Green (1997) provide equations to calculate the product of gas emissivity times a reference gas temperature since this product ($\varepsilon_{f,Tf}T_f$) changes less with temperature than emissivity alone does. The constants to evaluate this product depend on the gas composition, (in our case p_{H2O} / p_{CO2} = 2) as well as the reference temperature. The term $\varepsilon_{f,Tf}T_f$ is also a function of the product of the partial pressure of the radiating species (P_{rad} = p_{H2O} + p_{CO2}, atm) times the mean beam length of the flue gas (L_m, m). The two reference temperatures used were 727°C (Low) and 1227°C (High) since for most CV in the CHE, the flue gas temperature will be in that interval. This will be so for inlet flue gas temperatures of 1300°C or less. Thus for T_L = 727°C (1000K),

$$\log_{10}\varepsilon_{f,TL}T_L = 2.6367 + 0.2723\log P_{rad}L_m - 0.0804\log^2 P_{rad}L_m + 0.0030\log^3 P_{rad}L_m \tag{2.41}$$

and for $T_H = 1227°C$ (1500K),

$$\log_{10} \varepsilon_{f,TH} T_H = 2.7178 + 0.3386 \log P_{rad} L_m - 0.0990 \log^2 P_{rad} L_m - 0.0030 \log^3 P_{rad} L_m \quad (2.42)$$

Units are important: temperatures are reported in degrees Kelvin [K] and $P_{rad}L_m$ is in m-atm. By linear interpolation or extrapolation one may zero in on the flue gas temperature of interest:

$$\varepsilon_{f,Tf} T_f = \frac{[\varepsilon_{f,TH} T_H (P_{rad} L_m)](T_f - T_L) + [\varepsilon_{f,TL} T_L (P_{rad} L_m)](T_H - T_f)}{500} \quad (2.43)$$

where the brackets in the term [A(x)] indicate that the parentheses refer not to a multiplier but to an argument.

Gas absorptivity (from which the gas transmissivity may be obtained) depends both on the temperature of the flue gas and on the temperature of the surface at which the radiation was emitted. In the CV the two surface temperatures of interest are T_{s1} (wall) and T_{c2} (coiled tube). Gas absorptivities may be obtained from the constants for emissivities. Here the product $\alpha_{f,Ti}T_i$ (absorptivity of the gas times the temperature of the surface T_i from which the radiation was emitted) is equal to $\varepsilon_{f,Ti}T_i$ evaluated at T_i and not T_f and at $P_{rad}L_mT_i / T_f$ instead of $P_{rad}L_m$, and then multiplied by $(T_f / T_i)^{0.5}$. The exponent 0.5 is an adequate average of the exponents used to calculate the absorptivity of the pure components (CO_2: 0.65 and H_2O: 0.45). The product $\alpha_{f,Ti}T_i$ is evaluated at two reference temperatures (1000K and 1500K) for which there are constants available (those of the emissivity). Note that here the reference temperatures refer not to the flue gas temperature but to the surface temperature at which the radiation was emitted. For $T_L = 727°C$ (1000K),

$$\alpha_{f,TL} T_L = \left[\varepsilon_{f,TL} T_L \left(T_L, \frac{P_{rad} L_m T_L}{T_f} \right) \right] \left(\frac{T_f}{T_L} \right)^{0.5} \quad (2.44)$$

and for $T_H = 1227°C$ (1500K),

$$\alpha_{f,TH}T_H = \left[\varepsilon_{f,TH}T_H\left(T_H, \frac{P_{rad}L_mT_H}{T_f}\right)\right]\left(\frac{T_f}{T_H}\right)^{0.5} \tag{2.45}$$

Temperature terms are in degrees Kelvin [K], P_{rad} in atm and L_m in m. As in the case of the emissivities, the brackets in the term [A(x,y)] indicate that the parentheses refer not to a multiplier but to an argument. Since the reference temperatures for emissivity and transmissivity calculations happen to be the same, the constants to evaluate the term $\varepsilon_{f,TL}T_L$ in Eq. (2.44) are those of Eq. (2.41) and the constants for the term $\varepsilon_{f,TH}T_H$ in Eq. (2.45) appear in Eq. (2.42). As stated earlier, there exists a correction in the pressure-beam length term in the argument of the logarithm when calculating absorptivities. Linear interpolation or extrapolation allows one to evaluate the absorptivity at the appropriate surface temperature:

$$\alpha_{f,Ti}T_i = \frac{\alpha_{f,TH}T_H(T_i - T_L) + \alpha_{f,TL}T_L(T_H - T_i)}{500} \tag{2.46}$$

Finally, the transmissivity of the gas may be obtained from the absorptivity:

$$\tau_{f,Ti} = 1 - \alpha_{f,Ti} \tag{2.47}$$

Since the wall of the CV is assumed to be adiabatic, there is no net exchange by radiation between the flue gas and the wall or between the wall and the coiled tube itself (otherwise the wall would not be adiabatic). Thus in the CV the only net exchange of heat by radiation occurs between the flue gas and the coiled tube. As a result, for the purposes of the thermal circuit in Figure 2.5, the driving force for this exchange is conveniently expressed by the difference in temperature between the gas and the coiled tube ($T_f - T_{c2}$). The radiation flux q_{rc} in Eq. (2.34) is defined as a heat loss. Since the coiled tube actually receives heat, it is necessary to introduce a negative sign in the expression for the heat transfer coefficient by radiation ($W/m^2\,°C$):

$$h_{rc} = \frac{-q_{rc}}{T_f - T_{c2}} \tag{2.48}$$

2.2.6 Energy Balance Equations

After the analysis of §2.2.3 on the thermal circuit for each CV with the temperature driving force and resistance terms for all the heat transfer mechanisms between the flue gas and the oil and between the flue gas and the environment (losses), correlations and models were presented for the estimation of the heat transfer coefficients in §§2.2.4 and 2.2.5. The purpose of this section is to derive the governing equations for the temperature of the oil and flue gas streams and two important surface temperatures: on the outside of the coiled tube (T_{s2}) and on the inside of the stack (T_{s1}). This will allow one to calculate the heat gained by the oil and lost to the environment at each CV.

The CHE is designed with a counter-current configuration with the oil entering at the top. We assume that the oil temperature at the inlet of the CHE and the flue gas temperature at the outlet of the CHE are known as illustrated in Figure 2.11. The CHE is divided into a number of CV that each contains one full turn of the coiled tube. The first CV is at the top of the CHE at the oil inlet.

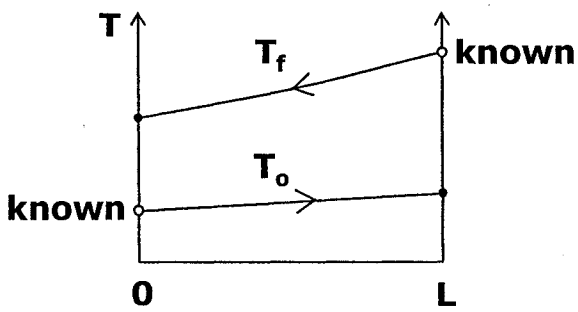

Figure 2.11 Schematic temperature profile of the oil and flue gas stream across the CHE in counter-current configuration.

The Well-Mixed assumption within each CV is applied to the oil and flue gas temperatures. These are assumed to change instantaneously upon entering each CV to attain their new steady state value. In heat transfer, the temperature difference between the two streams is more important than their individual values. By being consistent and using the same convention for the two streams and knowing that the oil does not change its temperature significantly, the assumption may be justified. Thus the temperature leaving a CV is the same as the bulk temperature in that CV (e.g., $T_{f,i}$). Likewise the temperature of the inlet stream to the i^{th} CV is the temperature of the previous CV (e.g., the flue gas temperature at the inlet of the i^{th} CV is $T_{f,i-1}$). Each CV is also defined by the surface temperatures of the coiled tube and insulated stack, i.e., T_c's and T_s's. These temperatures are assumed to be constant within each CV and change from one CV to the next. A schematic diagram of the CHE in terms of contiguous CV is shown in Figure 2.12.

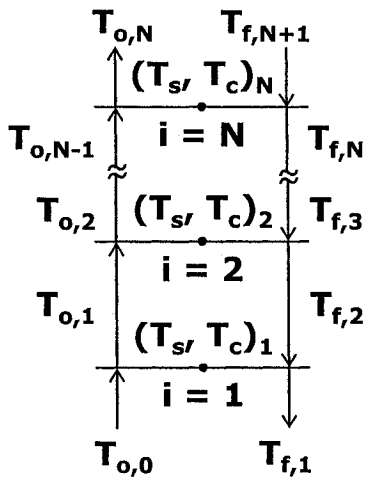

Figure 2.12 Schematic flow diagram of the CHE in terms of CV.

The solution of the CHE starts with the CV at the top and marches on towards the bottom of the CHE. At the top CV, the inlet temperature of the oil is known ($T_{o,0}$). Through an educated guess based on the known $T_{f,N+1}$ (the temperature of the flue gas at the bottom of the CHE) and the amount of heat that is exchanged between the oil and the flue gas (see §2.2.8), one may calculate the flue gas temperature leaving the top CV ($T_{f,1}$). Thus for the first CV, the oil temperature entering the CV and the flue gas temperature leaving the CV are

the only known values. The other temperatures have to be calculated. After solving the first CV, the unknowns of the first CV become the known variables of the second CV as far as the flue gas and oil temperatures are concerned. The surface temperatures of the first CV now known, will serve as the initial guess for those variables in the second CV. Known and unknown variables appear in Figure 2.13 where the dotted arrows indicate that a variable is an input to the CV.

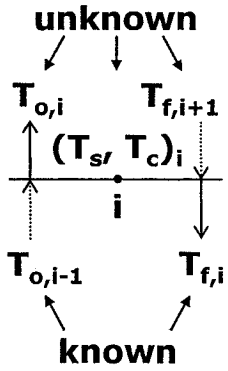

Figure 2.13 Schematic diagram of the temperatures that define the i^{th} CV and its inputs.

The analysis consists of two energy balances on the oil and flue gas streams and two surface balances on the outside of the coiled tube and the inside of the stack. All balances reflect steady state conditions. In the case of the oil and flue gas streams, the balance consists of equating the heat gained or lost by the oil or flue gas (represented by the $C_p\Delta T$ term) with the heat flow at an appropriate surface expressed by the ratio of the temperature driving force and the resistance to heat transfer. For example, in the OIL equation, the heat flow is expressed by the ratio of the temperature difference between the outside of the coiled tube and the oil itself. The resistance term R_{coil} accounts for two heat transfer mechanisms in series: conduction through the coiled tube and internal convection of the oil. In the case of the two surface balances only heat flows are equated. For instance, on the outside of the coiled tube the heat flow from the flue gas that is characterized by R_{fc} (a combination of radiation and external convection processes in parallel) and the $(T_f - T_{c2})$ driving force is equal to the heat flow represented by R_{coil} and $(T_{c2} - T_o)$. Resistance terms have been based either on the length of the coiled tube (Δx) in the CV or on the height of the CV ($b\Delta x/l_{turn}$) in

§2.2.3. These resistance terms are estimated a priori by guessing the surface temperatures and the oil temperature. The flue gas temperature is already a known variable in the CV and does not need to be guessed.

For the i^{th} CV the four energy balances are:

- OIL equation

$$M_o C_{Po}(T_{o,i} - T_{o,i-1}) = \frac{T_{c2} - T_{o,i}}{R_{coil}} \tag{2.49}$$

Known: M_o, $T_{o,i-1}$

Estimated: C_{Po}, R_{coil}

Unknown: $T_{o,i}$, T_{c2}

Note: both sides of the expression represent the heat gained by the oil in the CV (Q_{oil}). According to the Well-Mixed assumption, the oil heat capacity is evaluated at $T_{o,i}$ with the value of the previous iteration (see §2.2.8 for iterative procedure).

- FLUE GAS equation

Starting point:

$$M_f C_{pf}(T_{f,i} - T_{f,i+1}) = -Q_{oil} + Q_{loss} \tag{2.50}$$

where the left-hand side is negative (heat lost by the flue gas, Q_{flue}) and

$$Q_{oil} = \frac{T_{c2} - T_{o,i}}{R_{coil}} \tag{2.51}$$

$$Q_{loss} = \frac{T_e - T_{s1}}{R_{stack}} \tag{2.52}$$

By convention, Q_{loss} is defined as negative to indicate that heat flows out the stack. Combining the last three expressions

$$M_f C_{pf}(T_{f,i} - T_{f,i+1}) = -\frac{T_{c2} - T_{o,i}}{R_{coil}} + \frac{T_e - T_{s1}}{R_{stack}} \tag{2.53}$$

Known: M_f, C_{Pf}, $T_{f,i}$

Estimated: R_{coil}, R_{stack}

Unknown: $T_{o,i}$, T_{c2}, T_{s1}, $T_{f,i+1}$

Note: both sides of the expression represent the heat lost by the flue gas in the CV (Q_{flue}).

- COIL equation

  Starting point:

$$Q_{fc} = Q_{oil} \tag{2.54}$$

$$\frac{T_{f,i} - T_{c2}}{R_{fc}} = \frac{T_{c2} - T_{o,i}}{R_{coil}} \tag{2.55}$$

Known: $T_{f,i}$

Estimated: R_{fc}, R_{coil}

Unknown: $T_{o,i}$, T_{c2}

- STACK equation

  Starting point:

$$Q_{fs} = Q_{loss} \tag{2.56}$$

$$\frac{T_{s1} - T_{f,i}}{R_{fs}} = \frac{T_e - T_{s1}}{R_{stack}} \tag{2.57}$$

Known: $T_{f,i}$, T_e

Estimated: R_{fs}, R_{stack}

Unknown: T_{s1}

Table 2.1 summarises the known and unknown variables in the four balances.

Table 2.1 Summary of the governing equations for each CV and their unknowns.

Equation	**Unknowns**
OIL, Eq. (2.49)	$T_{o,i}$, T_{c2}
FLUE GAS, Eq. (2.53)	$T_{o,i}$, T_{c2}, T_{s1}, $T_{f,i+1}$
COIL, Eq. (2.55)	$T_{o,i}$, T_{c2}
STACK, Eq. (2.57)	T_{s1}

One strategy to solve for the four temperatures is as follows:

a) solve STACK for T_{s1}:

$$T_{s1} = \frac{R_{stack} T_{f,i} + R_{fs} T_e}{R_{stack} + R_{fs}} \tag{2.58}$$

b) rearrange OIL and COIL to give the following equations for $T_{o,i}$ and T_{c2} that are solved sequentially:

$$T_{o,i} = \frac{R_{coil} T_{f,i} + M_o C_{Po} R_{coil} (R_{fc} + R_{coil}) T_{o,i-1}}{R_{coil} + M_o C_{Po} R_{coil} (R_{fc} + R_{coil})} \tag{2.59}$$

$$T_{c2} = T_{o,i} + M_o C_{Po} R_{coil} (T_{o,i} - T_{o,i-1}) \tag{2.60}$$

c) solve FLUE GAS for $T_{f,i+1}$:

$$T_{f,i+1} = T_{f,i} + \frac{T_{c2} - T_{o,i}}{M_f C_{Pf} R_{coil}} - \frac{T_e - T_{s1}}{M_f C_{Pf} R_{stack}} \tag{2.61}$$

Note that these four variables ($T_{o,i}$, T_{c2}, T_{s1}, $T_{f,i+1}$) represent calculated and not guessed values. The final solution of each CV requires an iterative procedure since initially there are only guessed values of some of the variables (see §2.2.8). This procedure starts by guessing $T_{o,i}^*$ and the other variables (the asterisk in the superscript indicates a guessed value) and then compares it to the calculated value $T_{o,i}$ at the end of each iteration to check for convergence.

2.2.7 Temperature Profile and Heat Flux Equations

Temperature profile

The remaining surface temperatures (T_{c1}, T_{s2}, T_{s3} and T_{s4}) may be obtained from a series of energy balances. Knowing these temperatures helps in the calculation of variable property effects for h_{ci} (which requires T_{c1}), the thermal conductivity of materials and to foresee problems by checking the maximum service temperature of the construction materials.

The energy balances are based on the different ways of writing the temperature driving force and resistance to heat transfer ratio, so as to calculate the heat flow on any of the branches of the thermal circuit (see §2.2.3). The following equations are solved using the calculated values of $T_{o,i}$, T_{c2}, T_{s1}, $T_{f,i+1}$ and the original estimates of the resistance terms at the beginning of each iteration (several iterations are required to solve each CV).

- T_{c1} equation

  Starting point:

$$\frac{T_{c2}-T_{o,i}}{R_{coil}}=\frac{T_{c1}-T_{o,i}}{R_{hci}} \tag{2.62}$$

$$T_{c1}=T_{o,i}+\frac{R_{hci}(T_{c2}-T_{o,i})}{R_{coil}} \tag{2.63}$$

- T_{s2} equation

  Starting point:

$$\frac{T_e-T_{s1}}{R_{stack}}=\frac{T_e-T_{s2}}{R_{ins}+R_{jack}+R_{hso}} \tag{2.64}$$

$$T_{s2}=T_e-\frac{(R_{ins}+R_{jack}+R_{hso})\cdot(T_e-T_{s1})}{R_{stack}} \tag{2.65}$$

- T_{s3} equation

  Starting point:

$$\frac{T_e-T_{s1}}{R_{stack}}=\frac{T_e-T_{s3}}{R_{jack}+R_{hso}} \tag{2.66}$$

$$T_{s3}=T_e-\frac{(R_{jack}+R_{hso})\cdot(T_e-T_{s1})}{R_{stack}} \tag{2.67}$$

- T_{s4} equation

  Starting point:

$$\frac{T_e - T_{s1}}{R_{stack}} = \frac{T_e - T_{s4}}{R_{hso}} \tag{2.68}$$

$$T_{s4} = T_e - \frac{R_{hso}(T_e - T_{s1})}{R_{stack}} \tag{2.69}$$

Heat flux equations

In every CV the heat lost by the flue gas (Q_{flue}) is divided between the oil stream (Q_{oil}) and the heat losses to the environment (Q_{loss}). The terms Q_{flue} and Q_{loss} are reported as negative to indicate that heat is flowing out of the flue gas or out of the stack. Meanwhile Q_{oil} is positive since the oil temperature increases in every CV. These equations have been derived in §2.2.6. (See Eq. (2.49) for Q_{oil}, Eq. (2.52) for Q_{loss} and Eq. (2.50) for Q_{flue}). As in the case of the temperature profile, heat flux equations are solved using the calculated values of $T_{o,i}$, T_{c2}, T_{s1}, $T_{f,i+1}$ and the original estimates of the resistance terms at the beginning of each iteration (several iterations are required to solve each CV).

2.2.8 Mathematical Solution by the Implicit Method: Design and Performance Problems

Two types of problems are considered: the design scenario and the performance scenario. The design scenario involves solving for the length of the coiled tube given the inlet and outlet oil temperatures (specified by the client) as well as the inlet temperature of the flue gas. The performance scenario considers an existing CHE of fixed coiled tube length and solves for the outlet temperature of the oil stream given its inlet temperature and that of the flue gas.

The net effect of heat conduction and radiation between adjacent CV has been neglected through the Long Furnace assumption (see §2.2.5). Thus both scenarios are initial-value problems that may be solved by a one-way marching procedure with an implicit technique for each CV and a shooting method to zero in on the flue gas temperature at the

outlet. The solution of each CV is iterative by nature since it starts by guessing the outlet oil temperature and all of the surface temperatures.

The one-way marching procedure implies that we start by solving the first CV at the top of the CHE knowing $T_{o,0}$ and with an initial guess for $T_{f,1}$ and the surface temperatures. After some iterations this will yield $T_{o,1}$ and $T_{f,2}$ along with the correct surface temperatures thanks to the implicit technique. These values become the new inputs to solve the second CV. In this fashion the solution marches on until the desired $T_{o,N}$ is reached (design problem) or the last CV is solved for (performance problem). At that point we compare the calculated $T_{f,N+1}$ with the given value (the flue gas temperature at the bottom of the CHE). If the difference is significant, a new estimate of $T_{f,1}$ is obtained and the procedure repeated. In the spreadsheet developed for the model the values of the last iteration for each CV (i.e., the converged solution) appear on separate rows (see Appendix B). It was thus easy to try new estimates of $T_{f,1}$ until $T_{f,N+1}$ reached the desired value. The initial guess of $T_{f,1}$ may be calculated from an energy balance on the flue gas stream knowing $T_{f,N+1\ fixed}$ and assuming that $Q_{flue} \approx 1.1 Q_{oil}$ to account for heat losses.

However for the sake of completeness, the algorithm for the shooting technique to estimate new values of $T_{f,1}$ would involve calculating two pairs of ($T_{f,1\ guess}$, $T_{f,N+1\ calc}$) and interpolating or extrapolating for the next $T_{f,1}$ knowing $T_{f,N+1\ fixed}$. If the third $T_{f,N+1\ calc}$ is still significantly different from $T_{f,N+1\ fixed}$, the first ($T_{f,1\ guess}$, $T_{f,N+1\ calc}$) pair is dropped and the next $T_{f,1}$ is calculated from the two most recent ($T_{f,1\ guess}$, $T_{f,N+1\ calc}$) pairs.

The implicit technique for each CV

In an implicit technique, the variable of interest at the current CV is a function of other unknown variables in the same CV, which calls for a fixed-point iteration procedure. In an explicit technique, the variable of interest at the current CV depends on other variables from the previous CV and thus may be solved for directly without the above search procedure. Compared to an explicit technique the implicit technique allows for larger steps. In our case, steps are measured in terms of a fraction of the length of the coiled tube in one CV (e.g., ½ or the full length). The implicit technique may potentially lend itself to small

errors in the final value of the variable of interest (e.g., if the check for convergence is not done properly at every CV) whereas an explicit technique has greater chances of overshooting the final value unless a small enough step size is used (since it is the slope at the previous CV that is used to determine the current value).

In the present case, the implicit technique consists of guessing the outlet temperature of the oil and comparing it to the calculated value from solving the CV energy balance equations. Surface temperatures need to be guessed as well, which precludes the use of an explicit technique to solve the CHE. By comparing the calculated values of $T_{o,i}$ and T_{s1} with their guessed values under a certain tolerance level, one can decide if another iteration is needed to solve the CV. Heat fluxes and surface temperatures are also computed for each CV. For the first iteration of the i^{th} CV the initial guess of $T_{o,i}$ relies on the inlet temperature $T_{o,i-1}$ and the temperature increase from the previous CV (ΔT_o).

$$T_{o,i}^{*} = T_{o,i-1} + \beta \Delta T_o \tag{2.70}$$

where $\Delta T_o = T_{o,i-1} - T_{o,i-2}$ and β is a relaxation coefficient between 0 and 1, which is set to 1 in our case. For the first CV a reasonable guess of 1°C for ΔT_o was used. ΔT_o will change with the number of CV into which the CHE is divided.

The initial guess of the surface temperatures for the first CV does not need to be accurate since successive iterations will refine these values quickly. Rough estimates may be based on the flue gas and oil temperatures. For example, for the first CV, the inlet and outlet temperatures of the coiled tube may be set to 123.4°C (the oil temperature at the top of the CHE). The stack temperatures must fall between the flue gas temperature at the outlet ($T_{f,1}$) and the environment temperature. For subsequent CV (2, 3 ... N) the final values from the previous CV are used as initial guesses for the first iteration of the current CV. Within one CV the oil, flue gas and surface temperatures are refined as the iterations progress. The step-by-step implementation of the implicit technique is therefore as follows:

- Solving for the i^{th} CV

a) Inputs:

Known: $T_{f,i}$, $T_{o,i-1}$

Guess: T_c^*'s and T_s^*'s (use values from previous CV)

Guess: $T_{o,i}^*$ see Eq. (2.70)

b) With those inputs estimate R_{fc} from Eq. (2.6), R_{fs} from Eq. (2.7), R_{stack} from Eq. (2.12), and R_{coil} from Eq. (2.15). The expressions for the heat transfer coefficients may be found in §§2.2.4 and 2.2.5.

c) Solve for T_{s1} from Eq. (2.58); for $T_{o,i}$ from Eq. (2.59); for T_{c2} from Eq. (2.60); and for $T_{f,i+1}$ from Eq. (2.61). The last three equations are solved simultaneously using the values of $T_{o,i}$, T_{c2} and T_{s1} that are being calculated as opposed to the guessed values from step a). Use the resistance terms from step b).

d) Solve for T_{c1} from Eq. (2.63); for T_{s2} from Eq. (2.65); for T_{s3} from Eq. (2.67); for T_{s4} from Eq. (2.69); for Q_{oil} from Eq. (2.49); for Q_{loss} from Eq. (2.52); and for Q_{flue} from Eq. (2.50). Use the calculated values of $T_{o,i}$, T_{s1}, T_{c2}, and $T_{f,i+1}$ from step c) and the resistance terms from step b).

e) Compare: The current iteration is the last one for a CV when $|T_{o,i} - T_{o,i}^*| < 0.0002°C$ and $|T_{s1} - T_{s1}^*| < 0.1°C$. Checking for both conditions is considered to be a more reliable test. Since T_{s1} is the variable that changes the most from one it iteration to the next, once it has converged within 0.1°C, all the other temperature and heat flux terms are essentially constant.

f) If NO: Go back to step a). Instead of Eq. (2.70) use the following formula to update the guessed value of the oil temperature leaving the current CV.

$$T_{o,i\ next\ iter}^* = (1-\gamma)\, T_{o,i\ this\ iter} + \gamma T_{o,i\ this\ iter}^* \tag{2.71}$$

where the coefficient γ is set to 0 since in general convergence for a CV may be achieved in four or five iterations; i.e., the use of under-relaxation (i.e., γ between 0 and 1) is not required in this case. Update the guessed values of the surface temperatures (T_c^*'s and T_s^*'s) using the values from the iteration just completed.

g) If YES: At the i^{th} CV, the values $T_{o,i}$, $T_{f,i+1}$, T_{c1}, T_{c2}, T_{s1}, T_{s2}, T_{s3}, T_{s4}, Q_{oil}, Q_{loss}, and Q_{flue} have been established. Move to the next CV by using the following inputs in step a)

Known:

$$T_{f,i\,new\,CV} = T_{f,i+1\,old\,CV}$$

$$T_{o,i-1\,new\,CV} = T_{o,i\,old\,CV}$$

Guess: T_c^*'s and T_s^*'s (use values from the last iteration of the previous CV)

Guess: $T_{o,i}^*$ see Eq. (2.70)

The design scenario aims for the surface area of the coiled tube to accomplish a fixed rise in the oil temperature given the temperature of the flue gas stream at the bottom of the CHE. Thus the check point once a CV is solved is whether the exiting oil temperature from the CV is equal to 180°C. If not, a new CV should be added. If yes, check that the flue gas temperature entering the last CV ($T_{f,N+1}$) is reasonably close (within 5°C) to the given temperature of the flue gas stream at the bottom of the CHE. If not, $T_{f,1}$ can be adjusted manually or by a shooting method as explained above. Once $T_{f,N+1}$ and $T_{f,1}$ are in agreement, the total surface area of the CHE, in terms of the outer coiled tube surface, is simply the product of the surface area of the coiled tube in one CV times the number of CV required to reach the final oil temperature.

The performance scenario is concerned with the temperature of the oil at the bottom of the CHE when the oil temperature at the top and the flue gas temperature at the bottom of an existing CHE are known. The CHE is therefore divided into a known number of CV. Here the end point of the simulation is simply when the last CV is reached. It is still necessary to check for the right value of $T_{f,1}$ that yields the known $T_{f,N+1}$ as in the design problem. The oil temperature leaving the CHE is then recorded.

A spreadsheet in Excel has been designed to implement the implicit method (see Appendix A). The values of the last iteration for each CV (i.e., the converged solution) appear on separate rows so that all the important variables throughout the CHE are easily visualised (see Appendix B).

Finally, the solution to the design problem of the reference case involves choosing the thickness of insulation that minimises the heat loss to the environment while respecting the maximum service temperature of the stack material. The procedure to achieve this compromise and its final answer is presented in §3.4.1.

3 Results and Discussion

The objective of this chapter is to present and discuss the results obtained for the modelling of the combustion of solution gas in excess air, and the design and performance scenarios of the Coil Heat Exchanger. These results follow from the modelling methodology developed in §2 and the specifications for the client heat flow rate, the oil temperatures at the client inlet and outlet, the amount of solution gas available and its inlet temperature.

3.1 Combustion Calculations

In the reference case, solution gas was modelled as a stream of pure methane gas (CH_4) at STP (T = 0°C and P = 101 kPa) that reacts with air in a burner. The nominal flow rate of methane was 5.833×10^{-3} kg/s (21 kg/h) which is equivalent to 257 070 m^3/year. This flow rate is in the order of the mean volume flared or vented for all physical batteries in Alberta in 1999 (246 900 m^3/year). Combustion air was modelled as containing 21% oxygen (O_2) and 79% nitrogen (N_2) by volume with a molecular weight of 28.848 kg/kmol. It was supplied 25% in excess of the stoichiometric amount (i.e., λ_A = 1.25). The required amount of combustion air was determined to be 1.249×10^{-1} kg/s (9.704×10^{-2} m^3/s) for the feed and flue gas stream compositions given in Table 3.1. The mass flow rate of flue gas was 0.1307 kg/s.

Table 3.1 Composition of the flue gas stream for the reference case.

Species	Feed		Flue Gas	
	m^3/s (STP)	mole fraction	m^3/s (STP)	mole fraction
CH_4	8.15×10^{-3}	0.0775	0.00	0.00
O_2	20.38×10^{-3}	0.1937	4.08×10^{-3}	0.0387
N_2	76.66×10^{-3}	0.7288	76.66×10^{-3}	0.7288
CO_2	0.00	0.00	8.15×10^{-3}	0.0775
H_2O	0.00	0.00	16.30×10^{-3}	0.1550
TOTAL	105.2×10^{-3}	1	105.2×10^{-3}	1

Once the composition of the flue gas was known, the theoretical flame temperature (TFT) was calculated under adiabatic conditions. In our calculations, heat capacities of real gases at low pressures were approximated by those of ideal gases (Smith et al., 1996). For

the reference case, the TFT was calculated to be 1723°C. The temperature of the flue gas at the point of contact with the coil heat exchanger will be lower than the TFT due to radiative and convective thermal losses. Since the details of the burner were unknown a reasonable value for that flue gas temperature was assumed (see §3.3). The impact of the air number on the TFT and the volume of combustion air are presented in Figure 3.1.

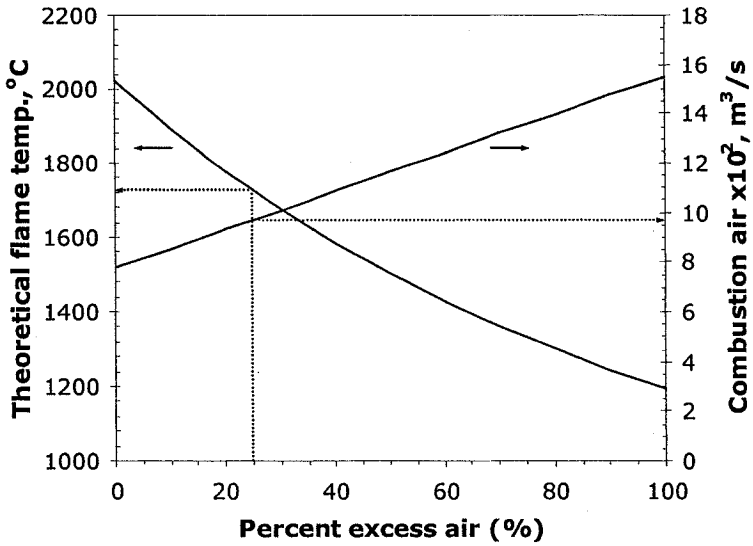

Figure 3.1 Effect of percent excess air on the TFT and the volumetric flow rate of combustion air.

3.2 Geometry of the Coil Heat Exchanger and Materials of Construction

The Coil Heat Exchanger (CHE) was modelled as having a counter-current configuration with the inlet of the oil stream at the top of the flare stack. The following geometrical details were chosen in accordance with typical dimensions of solution gas flares. The heat exchanger section was housed in a 25.4 cm-I.D. stack and consisted of a vertical helical coil with radius of curvature equal to 8.53 cm. The length of one turn of coiled tube

was 53.60 cm. The coiled tube's internal diameter was 2.54 cm and the wall thickness was 4 mm. The vertical clearance between two turns of the coiled tube was 2.54 cm, which resulted in a height per turn of 5.88 cm. The gap between the coiled tube and the stack wall was 2.50 cm. Some of these dimensions are represented in Figure 3.2.

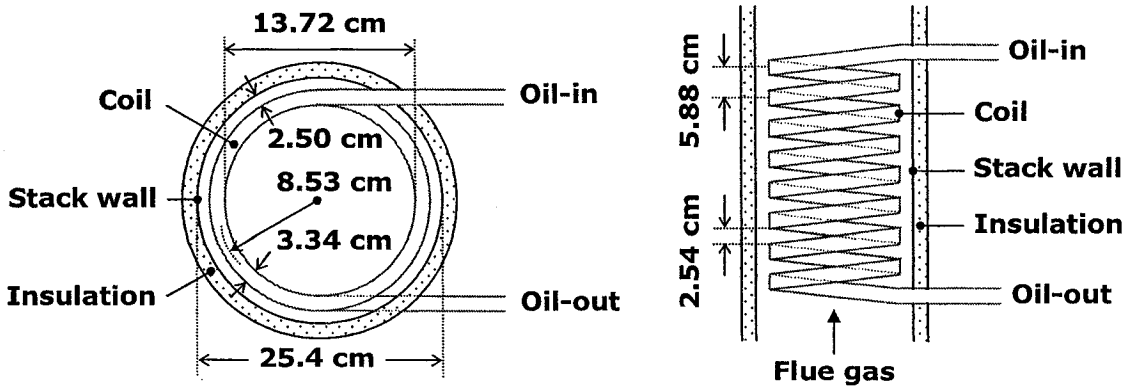

Figure 3.2 Plane and front view of the Coil Heat Exchanger (not to scale).

The recommended material of construction for the coiled tube and the stack was Stainless Steel 310 (25% Cr, 20% Ni, Bal. Fe), which allows for low intensity or occasional flame impingement and provides a good balance between cost and service life (Bussman et al., 1997; Perry and Green, 1997). The maximum service temperature in air of this austenitic chromium-nickel steel is 1035°C for intermittent operations and may reach 1150°C for continuous operations (MatWeb, 2004). Melting will occur in the range from 1400°C to 1455°C. It is also effective in resisting corrosion attack from sulphur-bearing streams such as hydrogen sulphide (H_2S) and sulphur oxides from sour gas flaring. For sour gases (H_2S > 10 ppm by volume), the use of high nickel alloys (e.g., Incoloy 800; composition: 21% Cr, 32% Ni, Bal. Fe) to protect against sulphidation attack on the coil and stack wall is discouraged (Bussman et al., 1997); instead, chromium is recommended as an alloying agent to resist sulphidation. Above 12% (by mass), chromium forms a self-healing and nonporous chromium oxide film (Edwards and Endean, 1995). When nickel is present, it diffuses through the chromium oxide layer and reacts with the sulphur environment to form nickel sulphides on top of the oxide layer. One of these sulphide components is Ni-Ni_3S_2, which melts at 635°C. The molten nickel sulphide can easily destroy the chromium oxide film and

lead to serious sulphidation attack. Another material considered was Stainless Steel 316 (18% Cr, 12% Ni, Bal. Fe) but its service temperature was lower than that of Stainless Steel 310. The composition of all the three metal alloys is taken from Perry and Green (1997).

The insulating material should withstand hot-side temperatures above 1000°C. Two types of products were considered: expanded silica (Perlite) and refractory fibres (Durablanket). Perlite is made from an inert siliceous volcanic rock that is expanded by heating above 535°C in order to remove the water content. This results in a cellular structure of minute air pockets surrounded by vitrified product. However commercially available Perlite insulation (e.g., Sproule® Perlite Insulation; see Extol, 2004) has a maximum service temperature below 700°C and thus was not retained as an option. The second material considered was Durablanket S® by Unifrax Corp. The line of cross-locked ceramic fibre products is available in different temperature grades, densities and sizes. The eight pound per cubic foot (8 PCF) blanket withstands temperatures up to 1280°C (Unifrax, 2002) and was therefore selected. A thickness of 1.27 cm was used as a result of the compromise between minimising heat losses and respecting the maximum service temperature of the stack material (see §3.4.1). The schematic diagram of the insulation system and its temperature profile are shown in Figure 3.3 (The coiled tube is not represented).

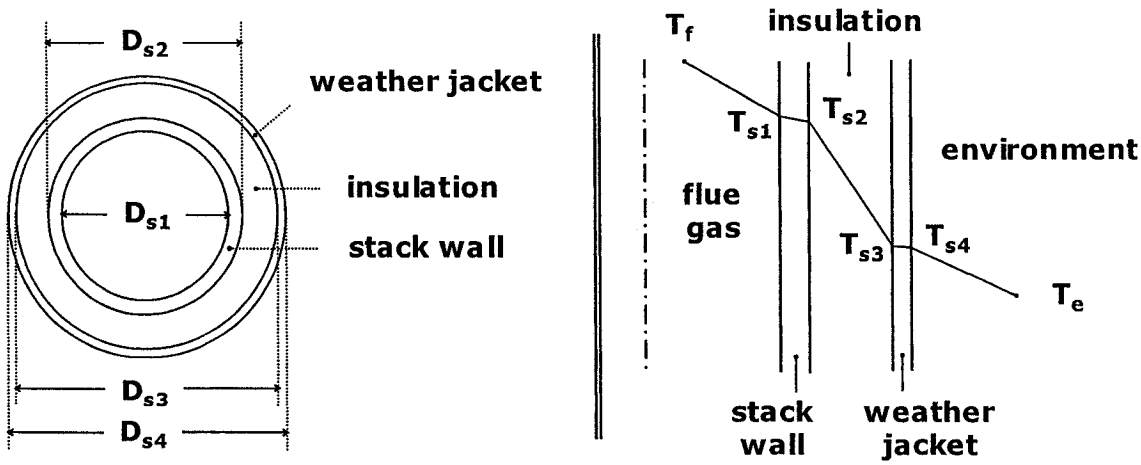

Figure 3.3 Geometry and temperature profile of the insulated stack (not to scale).

A weather jacket should cover the insulating material. Its aim is to prevent ambient moisture from increasing the effective thermal conductivity of the insulating material and protect against high winds and ultraviolet rays. The jacket was modelled as a 3 mm thick metal layer. A conservative value of the thermal conductivity (λ_{jack}) was set to 150 W/m°C. For comparison the thermal conductivity of aluminium at room temperature is 273 W/m°C (Perry and Green, 1997). The expected temperature range of the weather barrier was from 30°C (on a windy winter day with 0.1307 kg/s of flue gas at 1300°C) to 697°C (on a calm summer day with 0.2614 kg/s of flue gas at 1300°C). The choice of material for the weather jacket should take this temperature range into account.

The thermal conductivity as a function of temperature of Stainless Steel 310, Durablanket S and the weather jacket material appear in Table 3.2.

Table 3.2 Temperature correlations of the thermal conductivity of Stainless Steel 310, Durablanket 8 and weather jacket material. The range of applicability for the correlation is listed on the same row as the material's name. T in °C. The R^2 was higher than 0.99 in all cases.

STAINLESS STEEL 310[1]	[100°C – 500°C];
Thermal conductivity, W/m°C	$\lambda_{310} = 12.6345 + 0.0121T$
DURABLANKET 8[2]	[93°C – 982°C]
Thermal conductivity, W/m°C	$\lambda_{ins} = 5.201\text{x}10^{-2} + 3.2005\text{x}10^{-7}T^2 - 6.8289\text{x}10^{-6}T$
WEATHER JACKET	[30°C – 697°C]
Thermal conductivity, W/m°C	$\lambda_{jack} = 150$

1. see Perry and Green, 1997; 2. see Appendix A

3.3 The Reference Case: Flue Gas and Oil Streams

The calculation of the surface area of the CHE (design problem) was carried out for a set of material streams, geometrical configuration and dimensions and materials of construction that constitute the reference case. In this section, the nature of the oil stream is discussed and its thermo-physical properties and those of the flue gas stream are presented. The final list of all the elements of the reference case appears at the end.

The composition and flow rate of flue gas were derived in §3.1. These calculations were based on a stream of pure methane, simulating solution gas, burning to completion in 25% excess air. Since the details of the burner were unknown a value of 1300°C was assumed for the temperature of the flue gas at the point of contact with the coil (T-Flue-1 in Figure 2.2). This temperature, being lower than the TFT (1723°C) would account for radiation and convection thermal losses. The thermo-physical properties of the flue gas –heat capacity, density, thermal conductivity, kinematic and dynamic viscosities– were obtained from Hysys v3.0.1 (a software tool by Hyprotech Ltd), with the flue gas composition corresponding to that in Table 3.1 at atmospheric pressure. The property package selected in Hysys used the Peng-Robinson-Stryjeck-Vera equation of state. Temperature correlations of the flue gas properties appear in Table 3.3.

Table 3.3 Temperature correlations of the thermo-physical properties of the flue gas and oil streams. The range of applicability is listed by the stream's name unless otherwise stated. *T* in °C. The R^2 was higher than 0.99 in all cases.

FLUE GAS	[150°C – 1500°C]
Heat capacity, kJ/kg°C	$C_{Pf} = 1.1119 + 2.211x10^{-4}T$
Density[1], kg/m^3	$\rho_f = 0.5830 + 1.1064x10^{-7}T^2 - 4.2659x10^{-4}T$
Thermal conductivity, W/m°C	$\lambda_f = 1.9600x10^{-2} - 2.2080x10^{-8}T^2 + 8.3990x10^{-5}T$
Kinematic viscosity, m^2/s	$\nu_f = 1.403x10^{-5} + 1.0348x10^{-10}T^2 + 7.3198x10^{-8}T$
Dynamic viscosity, kg/m·s	$\eta_f = 1.6460x10^{-5} + 3.4441x10^{-8}T$
OIL	[104°C – 327°C]
Heat capacity, kJ/kg°C	$C_{Po} = 1.5924 + 0.0034T$
Density, kg/m^3	$\rho_o = 981.07 - 0.0005T^2 - 0.61T$
Thermal conductivity, W/m°C	$\lambda_o = 0.1228 - 1.3342x10^{-7}T^2 - 6.5899x10^{-5}T$
Kinematic viscosity, m^2/s	$\nu_o = 3.6261x10^{-6} - 1.2778x10^{-13}T^3 + 1.0770x10^{-10}T^2 - 3.1767x10^{-8}T$
Dynamic viscosity, kg/m·s	$\eta_o = 3.4434x10^{-3} - 1.2572x10^{-10}T^3 + 1.0545x10^{-7}T^2 - 3.0941x10^{-5}T$

1. Range of applicability [900°C – 1500°C]

The properties of the working fluid were those of Therminol®59 by Solutia, for which the optimum usable range is from -46°C to 316°C with a maximum film temperature of

345°C (Solutia, 1995). The ability to function at low temperatures is crucial for successful operation in the cold winter weather of Alberta where temperatures drop well below 0°C. This was the main reason why water was eliminated as a working fluid. The temperature correlations for the oil properties are shown in Table 3.3. According to the client unit's specifications (see §2.2.1), the oil temperatures at the inlet and outlet of the CHE had to be 123.4°C and 180°C, respectively. A required oil flow rate equal to 0.583 kg/s was calculated from Eq. (2.2).

The geometry and materials of construction of the coiled tube, the stack and the insulation system were discussed in §3.2. The listing of all the elements of the reference case is presented in Table 3.4.

Table 3.4 Elements of the reference case.

Solution Gas		**Coil Heat Exchanger**	
Composition	100% CH_4	Configuration	Counter-current
Mass flow rate, kg/s	5.833×10^{-3}	**Coiled Tube**	
Temperature and Pressure	STP	Material	Stainless Steel 310
Combustion Air		Inside diameter D_{cI}, m	25.4×10^{-3}
Mass flow rate, kg/s	1.249×10^{-1}	Other dimensions	see Figure 3.2
Temperature and Pressure	STP	**Stack**	
Air number	1.25	Material	Stainless Steel 310
Flue Gas		Inside diameter D_{sI}, m	0.254
Composition	see Table 3.1	Wall thickness, m	6×10^{-3}
Mass flow rate, kg/s	0.1307	**Insulation**	
T-Flue-1 (at the bottom of the CHE), °C	1300	Material	Durablanket 8
Oil		Outside diameter D_{s3}, m	0.3168
Composition	Therminol®59	Thickness, m	12.7×10^{-3}
Mass flow rate, kg/s	0.583	**Weather Jacket**	
T-Oil-6 (at the top of the CHE), °C	123.4	Thickness, m	3×10^{-3}
T-Oil-1 (at the bottom of the CHE), °C	180.0	Outside diameter D_{s4}, m	0.3228

3.4 Mathematical Solution of the Reference Case in the Design Scenario

This section contains the results and discussion of the design problem for the reference case. Firstly, the procedure to calculate simultaneously the proper thickness of insulation around the flare stack and the surface area of the coiled tube to meet client specifications is presented. Secondly, profiles of key variables like temperature, resistance to heat transfer and heat flows along the CHE are reported and discussed. These profiles allow one to compare the role played by each of the heat transfer mechanisms (e.g., radiation vs. convection) and to verify that the service temperature of construction materials has been respected. The last subsection explores how the final solution of the design problem is affected by changing the basis of the CV, i.e., the length of coiled tube in the CV unit. This analysis shows the versatility of the implicit method in solving the energy balance equations at each CV. The modelling methodology and mathematical solution for these results were presented in §2.2.

3.4.1 Surface Area of the Coil Heat Exchanger and Thickness of Insulation

The specifications for the client unit became those of the CHE under the no heat losses assumption for the oil loop in the heat recovery system (see Figure 2.2). Thus the temperature of the 0.583 kg/s oil stream should rise from 123.4°C to 180°C in the CHE, which represents an energy gain of 69.6kW. This energy, which corresponds to 23.8% of the net enthalpy of combustion of pure methane (see Perry and Green, 1997), was supplied by 0.1307 kg/s of flue gas at 1300°C.

The answer to the design problem of finding the coiled tube surface area was linked to the problem of finding the proper insulation thickness that balanced heat losses and the maximum service temperature of the stack. It may happen that adding too much insulation (e.g., 5 cm) while effectively reducing heat losses, sets the inner surface temperature of the

stack (T_{sl}) above the maximum service temperature of the stack material. The solution would be to decrease the thickness of insulation, thus reducing T_{sl} but increasing Q_{loss}. The compromise was resolved by looking for the thickness of insulation that minimised Q_{loss} while ensuring that T_{sl} was reasonably lower than the maximum service temperature of Stainless Steel 310.

Weather conditions and those of the flue gas stream had a great impact on T_{sl}. By increasing the mass flow rate of flue gas through the stack, the inner side of the stack wall became increasingly hotter. Similarly, a calm summer day yielded higher values of T_{sl} and lower heat losses, than a windy winter day. Summer weather conditions were modelled by setting $T_e = 30^oC$ and $h_{so} = 10$ W/m^{2o}C, the latter being the heat transfer coefficient of the air around the stack.

The weather conditions for the design problem of the reference case were those of a windy winter day ($T_e = -30^oC$, $h_{so} = 60$ W/m^{2o}C) since they would yield the highest heat losses (see the "design" box in Figure 3.4). It was decided to set the worst case scenario, i.e., the conditions that would result in the highest values of T_{sl}, as being those of a flue gas stream with doubled the flow rate in the reference case ($M_{f,max} = 2 \cdot M_{f,min} = 0.2614$ kg/s) and at the same temperature (1300°C) in calm summer conditions (see the "performance" box in Figure 3.4). Note that the reference flow rate is labelled with the "min" subscript to indicate that it is the cut-off flow rate at which the heat recovery system will be able to fulfill its mission once the area of the CHE has been fixed. At a lower flue gas flow rate than $M_{f,min}$, the oil stream would not reach 180°C in an existing CHE. In practice $M_{f,max}$ would depend on the capacity of the temperature control unit between the CHE and the client or on other measures to lower the flue gas temperature (e.g., by mixing the flue gas with cold air). The concern was that with a large enough $M_{f,max}$ the oil stream might overheat beyond the capacity of the control unit thus violating client specifications (see the parametric studies in §3.5.2).

The procedure to resolve the compromise was to determine the coiled tube surface area A_{co} from $M_{f,min}$ in WINTER conditions for a given thickness of insulation. The

temperature on the inside of the stack was recorded and compared with the maximum service temperature of the steel (1035°C for intermittent operation and 1150°C for continuous operation). The highest values of T_{s1} occurred at the bottom of the CHE where the flue gas comes in direct contact with the exchanger. If this temperature was below the service temperature of steel, another simulation was done with $M_{f,max}$ in SUMMER conditions. Similarly the highest value of T_{s1} was compared to the service limit and if T_{s1} was still lower than the limit, the amount of the insulation was increased. If the simulation predicted a higher value of T_{s1} than the service limit, the thickness of insulation was decreased before a new simulation started. Since the thickness of Durablanket 8 insulation is available in multiples of half an inch, only discrete values were used in our study. The chart of Figure 3.4 illustrates the procedure.

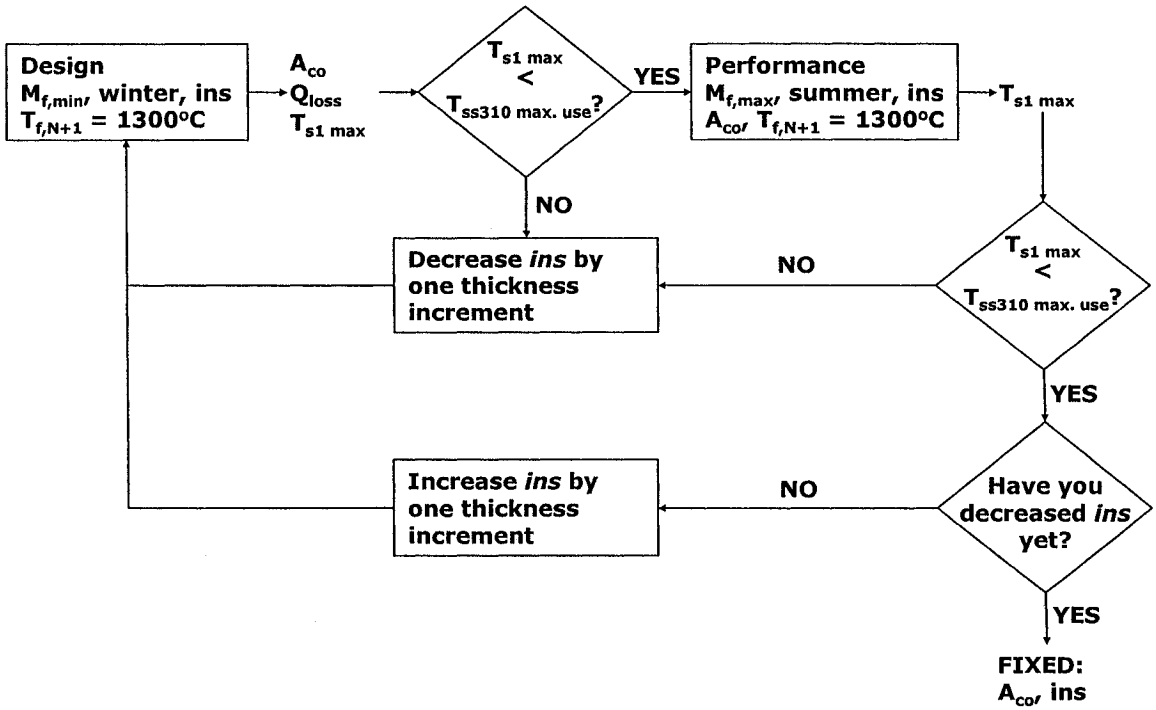

Figure 3.4 Procedure to calculate surface area of the coiled tube and the thickness of insulation (*ins*) in order to minimize heat losses while respecting the maximum service temperature of the stack material (Stainless Steel 310).

The analysis showed that the design outer surface area of the coiled tube was 1.181 m^2 for $M_{f,min}$ and WINTER conditions. The oil temperature at the bottom of the CHE was

181°C, slightly above the target of 180°C. The surface area translated into 21 turns of the coiled tube and the height of the CHE was 1.23 m. The optimal insulation thickness was 1.27 cm (one half of an inch). With this thickness and $M_{f,max}$ in a calm summer day, the inner side of the stack wall reached 1020°C, which was below the service temperature of Stainless Steel 310. Even though this value was close to the intermittent service limit (1035°C) it is important to realise that heat transfer to the stack wall (and therefore T_{s1}) has been overestimated by the assumption of the flue gas velocity in the gap between the coiled tube and the stack (see §2.2.4). For the reference flow rate, the inner stack temperature varied between 833°C in winter and 903°C in summer. Similarly the heat losses in winter conditions were 7.78% of the heat absorbed by the oil (70.9 kW) and decreased to 6.56% of Q_{oil} (71.4 kW) in summer conditions.

Finally, the effect of the two flow rates of flue gas on the temperature profile across the CHE may be easily visualised in Figure 3.5.

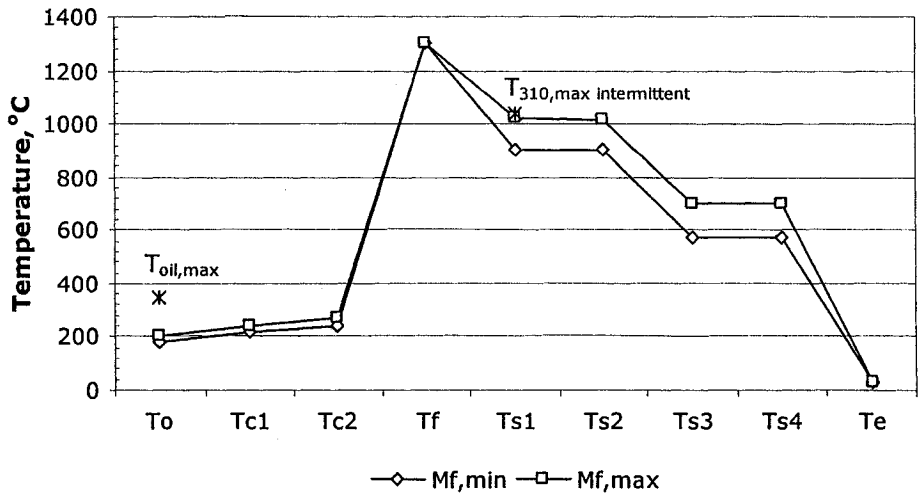

Figure 3.5 Highest profile of oil, flue gas and surface temperatures at the bottom of the CHE for two flue gas flow rates in summer conditions. The coil surface area was fixed at 1.181 m^2 and $M_{f,max} = 2 \cdot M_{f,min} = 0.2614$ kg/s. The maximum service temperature of Stainless Steel 310 for intermittent operation is 1035°C and the maximum bulk temperature of the oil is 345°C.

Both simulations represent summer conditions and an existing CHE with the same surface area A_{co} and insulation thickness as in the reference case. The maximum service temperature of the steel and the oil are above the figures predicted by the model. All values refer to the CV at the bottom of the CHE where the highest temperatures are achieved.

The difference in the oil temperature is significant from the control point of view. In the case of $M_{f,min}$, the oil temperature is 181.3°C (close to target) whereas for $M_{f,max}$ the oil exits the CHE at 203.6°C which is well above client specifications, hence the need for the control unit between the CHE and the client (see Figure 1.1). This performance scenario was explored in more detail in §3.5.2.

3.4.2 Local Variables along the CHE: Analysis of the Reference Case

The spreadsheet developed to solve the CHE allowed visualising the final answer of the implicit method for each CV. The available information includes, amongst others, temperature, heat transfer resistance and heat flux terms which define a contiguous series of thermal circuits (one for each CV). The full solution of the reference case appears in Appendix B. The aim of this section is also to verify some of the assumptions in the modelling methodology (including material properties) and to compare the influence of the modes of heat transfer between the flue gas and the oil. All this is done with data from the solution of the reference case solved in winter conditions.

Heat transfer mechanisms are conveniently represented in a thermal circuit that relates heat flow [kW] and temperature differences [°C] through the concept of the resistance to heat transfer [°C/kW]. Figure 3.6 shows the solution of the thermal circuit in the middle of the CHE (CV = 11, out of 21).

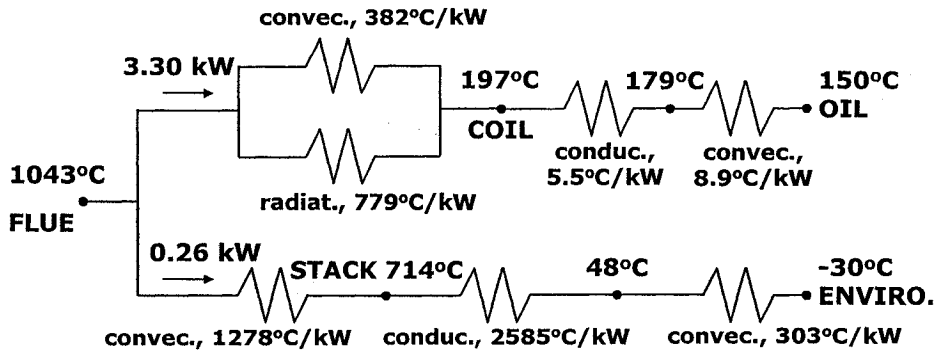

Figure 3.6 Thermal circuit for the middle CV in the CHE under reference case conditions (see Table 3.4).

In order to appreciate better the progression of these variables along the CHE, summary graphs were generated (see Figure 3.7). In these profiles, CV = 1 is at the top of the CHE where the oil enters.

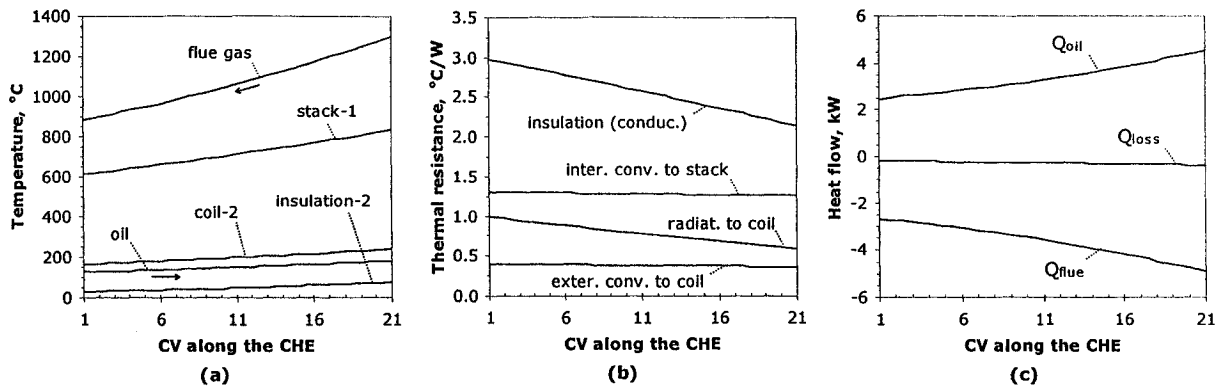

Figure 3.7 Key temperature, thermal resistance and heat flow terms along the CHE for the reference case in winter conditions. Graph (a): 1 = inside surface, 2 = outside surface.

Gas-side processes dominated the heat flow rate to the oil. For the middle CV, the resistance due to internal convection of the oil was only 2.36% of the convection resistance of the flue gas on the outside of the coiled tube. The middle CV was chosen for this comparison since both resistances decreased only slightly. Comparing the two mechanisms on the outside of the coiled tube surface, the radiation resistance was always larger than the

convection resistance: the ratio of radiation to convection resistances was 2.49 at the top of the CHE and 1.66 at the bottom. The radiation resistance decreased faster than the convection resistance as the temperature profile reached its maximum at the bottom of the CHE (where the flue gas enters). The marked decrease in radiation resistance versus the steadiness of the convection resistance was the reason why the oil heat flow was higher at the bottom of the CHE than at the top (see Figure 3.7 (c)). In this regard, the ratio of the inverse of the radiation resistance at the top and at the bottom was 0.61, which was similar to the ratio of the oil heat flow between those two points (= 0.54). (The inverse of the radiation resistance is directly proportional to the heat flow by radiation).

Heat losses to the environment were controlled by the insulation resistance that was always higher than the resistance due to internal convection of the flue gas in the stack (see the top two lines in Figure 3.7 (b)). As the temperature of the insulation material rose near the bottom of the CHE, its thermal conductivity increased allowing more heat to flow through it. Thus the resistance to heat transfer decreased. This increase in the heat flow through the insulation material may also be seen in the slight increase in heat losses at the bottom of the CHE (see Figure 3.7 (c)). The total heat losses (5.53 kW) represented 7.79% of the heat absorbed by the oil in the CHE (71.0 kW) when a blanket of 1.27 cm of insulation surrounded the stack. Heat losses may not be decreased further by adding insulation without the risk of increasing the temperature of the stack wall beyond its maximum service temperature at higher flue gas flow rates (see §3.4.1). Finally, note that since the mean wall temperature of the stack in the simulation was well above 500°C, we had to extrapolate from the temperature range of the thermal conductivity of Stainless Steel 310 found in Table 3.2. Since the dominating resistance was that of the insulating material (more than two orders of magnitude larger than the stack wall's), the inaccuracy incurred by this extrapolation is expected to be minor.

Heat conduction through construction materials was significant in the case of the insulation blanket and less so, in the coiled tube. The role of insulation was discussed in the previous paragraph. The temperature difference between the two sides of the coiled tube

ranged from 13.9°C at the top of the CHE and 24.1°C at the bottom, which was consistent with the higher heat flow and slightly lower conduction resistance at the bottom of the CHE.

The model was successful in implementing the radiation processes according to the assumptions in §2.2.5. View factor F_{ss} (from the wall or "stack" to itself) was 0.6207 and F_{sc} (from the wall to the coiled tube) was 0.3793 based on CV dimensions D_{s1} = 25.4 cm, D_{c2} = 3.34 cm, b = 5.88 cm and Δx = 0.536 cm. Similarly the value of the mean beam length L_m in Eq. (2.40) was 5.9 cm. Being rather low, it was expected that the radiation properties of the flue gas would not be significant in the radiation exchange equations, i.e., that the flue gas would behave more like a transparent medium for radiation. In fact, the average emissivity of the flue gas ($\varepsilon_{f,Tf}$) was 0.047 (maximum 0.057 at the top of the CHE), the average transmissivity associated with T_{s1} ($\tau_{f,Ts1}$) was 0.933 (maximum 0.943 at the bottom) and the average transmissivity associated with T_{c2} ($\tau_{f,Tc2}$) was 0.846 (maximum 0.862 at the bottom). Thus the irradiation arriving at the coiled tube surface (G_c) and at the wall of the CV (G_s) was dominated by the radiosity from the other surfaces ($F_{ji}\tau_{f,Tj}J_j$) and less so by the radiation of the flue gas itself ($F_{ji}\varepsilon_{f,Tf}\sigma T_f^4$) as Figure 3.8 shows.

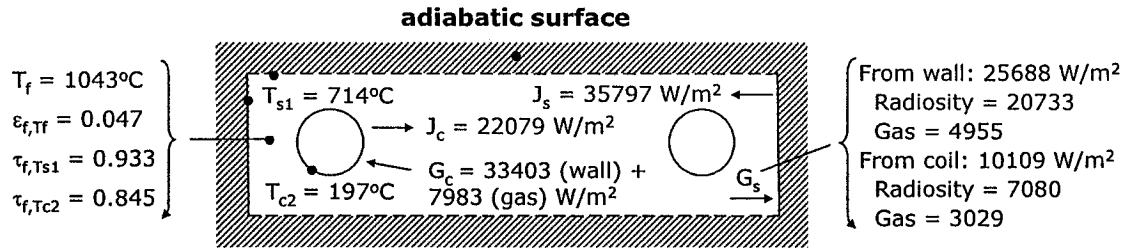

Figure 3.8 Radiation exchange between the coiled tube and the wall of the CV in the middle of the CHE (CV = 11).

Other observations can be drawn from Figure 3.8. The assumption about the wall of the CV being adiabatic was fulfilled: the irradiation on the wall stemming from the wall itself and from the coiled tube (and their corresponding gas radiation terms), was equal to the radiosity leaving the wall (J_s). The irradiation on the coiled tube was greater than its radiosity, which resulted in a negative net heat loss, i.e., a positive heat flux into the coiled

tube. Since the view factor from the coiled tube to itself was assumed to be zero, the irradiation on its surface came only from the wall of the CV. This assumption (that coiled tube did not see itself), yielded the maximum amount of heat that the coiled tube might receive by radiation. Therefore the current model represents an upper limit for the influence of radiation processes as far as view factors are concerned. The reason is that under this assumption the coiled tube was completely surrounded by surfaces at a higher temperature (T_{s1}) than its own (T_{c2}), when in reality the environment of the coiled tube consisted also of its own surface.

Finally, it is important to discuss the model assumptions. Reynolds and Prandtl numbers of the flue gas and oil streams appear in Table 3.5. All of them agreed with the limits of the Nusselt number correlations used in the modelling of convective processes (see §2.2.4). The total height of the CHE was 1.23 m. Since the internal diameter of the stack was 0.254 m, the ratio $H/D_{s1} = 4.8$ was close the expected value of 5. This ratio had been used to determine the entrance-effects correction factor for the convective heat transfer coefficient of the flue gas in the gap between the coiled tube and the stack (see §2.2.4). For the parametric studies of §3.5.1 –where the length of the coiled tube varies with different flue gas flow rates and temperatures– this correction factor was not modified for the sake of simplicity. Regarding the internal convection of the oil, the variable property correction factor for the Nusselt number in Eq. (2.22) was calculated at every CV. For all practical purposes it remained equal to approximately 1.03, indicating only a 3% increase in the Nusselt number. Its influence mattered little since it was gas-side and not oil-side processes that controlled the heat flow to the oil.

Table 3.5 Reynolds and Prandtl numbers for the oil and flue gas streams along the CHE.

	Reynolds number			**Prandtl number**		
Stream	Ave.	Top	Bottom	Ave.	Top	Bottom
Flue gas over coiled tube	2410	2769	2069	0.75	0.74	0.77
Flue gas relative to inside of stack	12 516	14 242	10 867	0.85	0.80	0.93
Oil in coiled tube	39 813	30 086	52 866	14.4	17.5	11.5

3.4.3 Effect of the Control Volume Size on the Solution to the Model

The basis of the definition of the CV was one full turn of coiled tube, i.e., $\Delta x = l_{turn}$. This choice determined the surface area of coiled tube in the CV, the height of the CV and other variables (e.g., view factors and the mean beam length of flue gas). On the former two dimensions rest the definitions of the heat resistance terms in §2.2.3. The logic behind the basis of the CV as one full length was simply to end up with an integer number of turns of coiled tube as the solution of the model. However all the equations in §§2.2.3 and 2.2.5 where the basis of the CV appeared, were left in terms of Δx and l_{turn}, without cancelling these terms out. The spreadsheet "CHE Simulator" respected this convention, which allows for cases where Δx is different from l_{turn}. When introducing the implicit technique of solving the energy balance equations for each CV (see §2.2.8), it was stated that this technique allowed for larger steps in terms of Δx than an explicit technique would. Due to the central role of Δx and in order to test the versatility of the implicit technique, the reference case under winter conditions was solved using four fractions of l_{turn} (⅛, ¼, ½ and ¾) as the basis of the CV. Results appear in Figure 3.9.

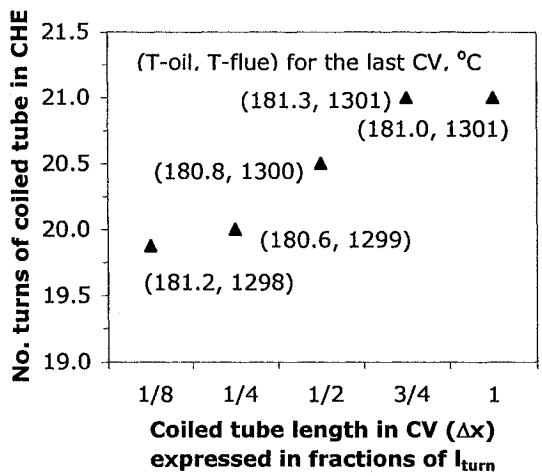

Figure 3.9 Solution of the reference case in winter conditions expressed in terms of the total number of turns of the coiled tube in the CHE for different lengths of the coiled tube as the basis of the CV (Δx = ⅛, ¼, ½, ¾ and one full turn of the coiled tube; l_{turn} = 53.60 cm).

Practically speaking, the difference between choosing ⅛ or one full turn of the coiled tube was only one turn more in the second case ($\Delta x = l_{turn}$). Although results were very similar, it seemed more conservative to base the simulation on one full turn and report the final answer as 21 turns. Flue gas, oil and surface temperatures were also very close. The inside temperature of the stack (T_{sI}) varied the most. By spreading the temperature difference over one extra coil turn, T_{sI} was higher by less than 10°C for ⅛ compared to the full length case. As a corollary, it might be said that the accuracy of the model from the point of view of the implicit technique, is plus or minus one turn of the coiled tube.

3.5 Parametric Studies of the Design and Performance Problems

After analysing the results for the reference case and checking the validity of the model assumptions, the model was used to solve the design and performance problems for different flue gas conditions. The design problem that seeks the area of heat transfer was extended to other flue gas flow rates and inlet temperatures than those in the reference case. Similarly the performance problem that predicts the outlet oil temperature from an existing CHE provided useful information for the design of the control unit and the range of flue gas flow rates that the CHE might handle safely.

3.5.1 Effect of Temperature and Mass Flow Rate of the Flue Gas on the Coiled Tube Surface Area

The inputs to the design problem are the inlet conditions of the material streams, the required heat flow rate and the basic geometry of the CHE. From these variables, the current model calculated the area for heat transfer expressed in terms of the outside surface area of the coiled tube in the CHE. By changing the flue gas flow rate and inlet temperature and keeping the heat flow rate and oil conditions the same, the model could be applied to oil and bitumen batteries of different sizes. More importantly since the reference case used a guessed

inlet temperature of the flue gas (1300°C), this temperature was chosen as the independent variable in Figure 3.10.

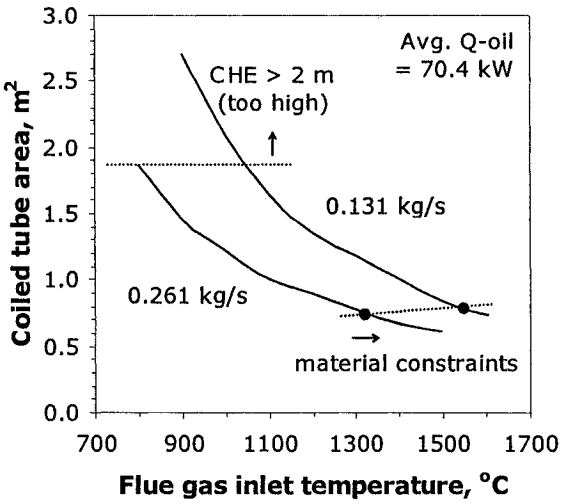

Figure 3.10 Effect of flue gas temperature (at the bottom of the CHE) and flow rate on the outside surface area of the coiled tube required to meet client specifications in summer conditions. The temperature of the 0.583 kg/s oil stream rises from 123.4°C to an average of 180.5°C.

Figure 3.10 shows that design calculations depended strongly on the inlet flue gas temperature and the mass flow rate of the flue gas. For a flue gas temperature of 1400°C, the required surface area would be 14.3% lower than in the 1300°C case. Alternatively if the flue gas were at 1100°C, the area would increase by 38.1% with respect to the reference case. Notice that once the area is fixed, the incoming flue gas temperature represents a lower limit below which the oil stream at 123.4°C will no longer reach the target value of 180°C. It may be referred to as the minimum flue gas temperature ($T_{f,min}$). In practice this lower limit should be the minimum temperature of the flue gas stream under analysis.

The mass flow rate of flue gas also played an important role in determining the area required for heat transfer. For the same incoming temperature of 1300°C, doubling the flue gas flow rate from the reference case of 0.1307 kg/s to 0.2614 kg/s would decrease the heat transfer area A_{co} by 33.4% (from 1.181 m^2 to 0.787 m^2).

Two natural boundaries appear in Figure 3.10. As the area for heat transfer increased due to lower flow rates and/or inlet temperatures of the flue gas, the height of the CHE increased. Once it reached two meters it was considered an unpractical solution due to its bulkiness. Pressure drop considerations and the capacity of the burner blowers might require an even smaller height. The second limit refers to the material of construction of the stack. At a certain flue gas temperature –different for each flow rate– the inside of the stack (T_{sl}) reached the lower of the two maximum service temperatures of Stainless Steel 310 (1035°C for intermittent operation). Beyond this point, structural damage of the steel will occur. It was interesting to note that the cut-off points were influenced significantly by the weather. Since T_{sl} was always higher in summer than in winter conditions, results were reported for the summer as the worst-case scenario. Summer conditions were T_e = 30°C and h_{so} = 10 W/m^{2o}C. For example, for 0.1307 kg/s with a flue gas inlet temperature of 1600°C, the maximum T_{sl} (at the bottom of the CHE) was 960°C in winter conditions, whereas in the summer, T_{sl} reached 1038°C when the flue gas entered at 1548°C.

3.5.2 Effect of Temperature and Mass Flow Rate of the Flue Gas on the Heat Absorbed by the Oil

Once the coiled tube surface area A_{co} was already set based on the flow rate and minimum temperature of the flue gas, it was useful to know the oil temperature at the outlet of the CHE with changes in the mass flow rate and temperature of the flue gas. This was the performance problem. Since there is a target temperature for the oil stream entering the client unit of 180°C, the amount of heat needed to be removed at the control unit (see Figure 1.1) could be calculated in cases where the oil temperature leaving the CHE was higher than the client's target. The two simulations consisted in running the reference case model for various flue gas inlet temperatures at two flue gas flow rates (0.1307 kg/s and 0.2614 kg/s) in summer conditions (worst case scenario where construction materials constraints will appear). The heat flow at the control unit was calculated as the heat absorbed by the oil in the existing CHE minus the design heat flow rate (69.6 kW). Results are shown in Figure 3.11.

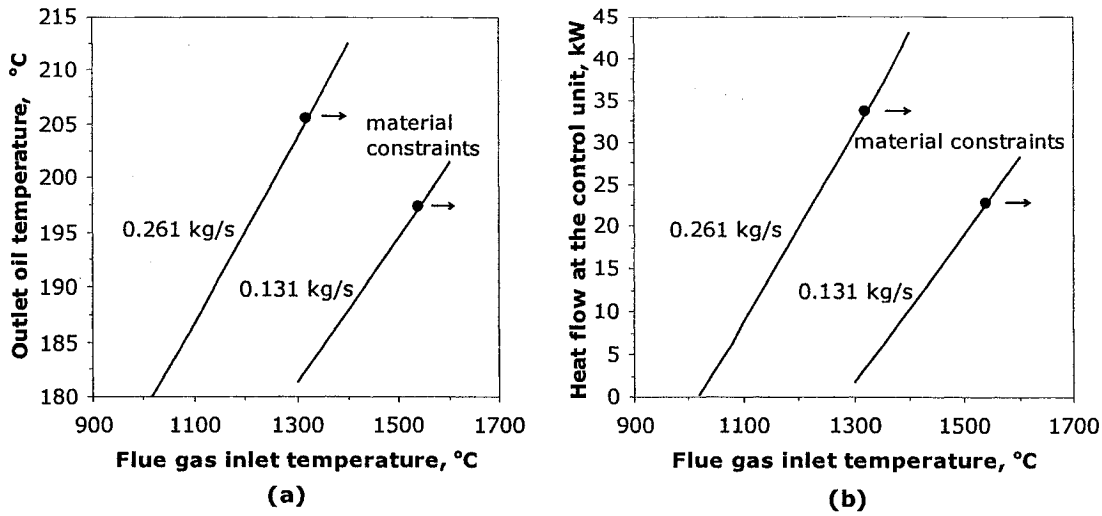

Figure 3.11 Effect of flue gas temperature and flow rate on the oil temperature at the outlet of the CHE (a), and on the heat flow to be removed from the oil at the control unit (b) in summer conditions. The coiled tube surface area was 1.181 m^2 and the inlet temperature of the 0.583 kg/s oil stream was 123.4°C.

The significant effect of flue gas conditions on the oil stream is readily observed. For instance, with a flue gas temperature of 1400°C, the outlet oil temperature rose to 187.8°C and it was necessary to remove 10.2 kW from the oil stream at the control unit to decrease its temperature back to target. If the mass flow rate of flue gas doubled, the minimum flue gas temperature dropped to 1018°C (instead of 1300°C at a flow rate of 0.1307 kg/s). Similarly for flue gas at 0.2614 kg/s and 1100°C, the exit oil temperature was 186.6°C and the control unit would remove 8.8 kW.

As in the design scenario, material problems arose when the inside temperature of the stack (T_{sI}) reached the lower of the two maximum service temperatures of Stainless Steel 310 (1035°C for intermittent operation). For the flue gas flow rate in the reference case (0.1307 kg/s), the cut-off inlet temperature of the flue gas was 1541°C and for 0.2614 kg/s, this temperature was 1322°C. These values were obtained in summer conditions in order to provide more conservative limits.

The performance scenario results provided some insight into the operating conditions of the heat recovery unit and its control strategy. It is clear that the CHE should not operate at the flue gas flow rate and inlet temperature of the reference case. In real life, any downward deviation from those conditions would result in an exit oil temperature lower than the target of 180°C. Therefore while the reference case was rightly used in the design calculations, the CHE should normally operate at higher flow rates (or inlet temperatures) of flue gas than in the reference case. This implies that the control unit as presented in Figure 1.1 is constantly removing heat from the oil. The sizing of this unit would depend on the expected range of flue gas flow rates and an average flue gas inlet temperature. By doubling the flue gas flow rate in the CHE with fixed A_{co} from the reference case conditions, the cut-off inlet temperature of the flue gas to avoid material problems was just above 1300°C (the value of the reference case) and the oil stream was overheated by 31 kW. Thus even though the control unit may be sized to remove that amount of heat, construction materials considerations require a second control option for operating at higher flow rates. This second strategy would involve injecting ambient air into the stack below the CHE or in the gap between the coiled tube and the stack in order to decrease the flue gas temperature at higher flue gas flow rates.

4 Conclusion and Recommendations

4.1 Conclusion

The following statements provide a summary of the background findings for the current work:

1. The heat recovery unit is best suited to oil and bitumen batteries that handle stable flow rates of solution gas. The best available data from the AEUB are monthly reports of the flow rate processed at a site. By good fortune, larger batteries tend to have more stable monthly flow rates.
2. The reference case was built around the average flow rate of solution gas flared or vented at an oil or bitumen battery in Alberta in 1999.
3. There is no data on the composition of solution gas flared or vented at the battery level, only for some individual wells. Since the inlet temperature of the flue gas was assumed to be 1300°C, composition of solution gas was not crucial for this project. However it will be important for the design of the burner section.
4. The ultimate objective of the recovery system is the generation of electricity to inject enough air for the complete combustion of solution gas that is flared in order to reduce greenhouse gas emissions and smoke formation.
5. The heart of the heat recovery unit is the counter-current, coil heat exchanger (CHE) where the oil stream recovers partially the thermal energy of the flue gas. The design problem consisted in calculating the outside surface area of the coiled tube given the client specifications on the oil stream (temperature increase and heat flow rate).
6. Geometry and choice of materials of construction for the heat recovery system were addressed keeping in mind the average dimensions of flare stacks and the maximum service temperature of the materials. The possibility of adding extended heat transfer surfaces on the CHE (e.g., fins) was discarded due to potential manufacturing issues.
7. The heat transfer model included temperature correlations of the thermo-physical properties of material streams (oil and flue gas) and materials of construction.
8. The model was based on the thermal circuit among the flue gas, the oil and the ambient air, and accounted for heat losses. The CHE was divided into cylindrical CV containing one full turn of the coiled tube. The thermal circuit at each CV was solved by an

implicit technique allowing for easy visualisation of key parameters (temperature, thermal resistance and heat flow) along the CHE.

9. The flexibility of the model lies in the distinction between the resistance to heat transfer terms and the actual heat transfer coefficients. The latter were obtained from standard convective heat transfer correlations and from the analysis of radiation exchange between grey surfaces in the presence of a radiating gas. Conduction was relevant in the case of the insulation around the stack and, to a lesser extent, in the case of the coiled tube.

10. For the reference case the outer surface area of the coiled tube was 1.181 m^2 (21 turns of the coiled tube) setting the height of the CHE at 1.23 m. The outer diameter of the insulated stack was 0.3228 m.

On the basis of the modelling of the CHE, the following conclusions may be drawn:

1. The heat transfer to the oil was controlled by gas-side processes (convection and radiation). The heat flow due to radiation increased noticeably at the bottom of the CHE (where the flue gas entered) increasing the oil heat flow in this region. The heat flow due to convection was fairly stable along the CHE.

2. The implicit technique to solve the steady state energy balance equations for each CV gave very similar results for different step sizes. The accuracy of the implicit technique was plus or minus one turn of the coiled tube.

3. The flow rate and inlet temperature of the flue gas in the reference case defined the minimum operating conditions of the CHE once the area for heat transfer was fixed. Operating at a lower flow rate and inlet temperature would prevent the oil from reaching its target temperature. Therefore the heat recovery unit should operate at a flow rate higher than that of the reference case while keeping the same inlet temperature of the flue gas.

4. The upper limit for the maximum flow rate of flue gas should be determined by the maximum service temperature of the stack material and by the capacity of the control unit to remove heat from the oil stream. Apart from the heat exchanger of the control unit, another strategy would be to mix cold ambient air with the flue gas, thus reducing the latter's inlet temperature at the point of contact with the coiled tube.

5. The flue gas conditions of the reference case (0.1307 kg/s, 1300°C) were extended in the parametric studies of the design scenario and the performance scenario. The latter looked at the outlet temperature of the oil stream entering at 123°C when the flue gas flow rate or its inlet temperature, were increased. The simulations for both scenarios showed the key role of flue gas properties on the area for heat transfer and on the outlet temperature of the oil in an existing CHE.

4.2 Recommendations

To further the work presented here, the following recommendations are made:

1. The implementation of the heat recovery unit is site-specific and requires information on the daily gas flow rates and its composition.
2. The burner unit should achieve complete combustion in order to reduce greenhouse gas emissions from the battery site. The size of the air blower(s) should make allowance for the pressure drop of the flue gas along the heat recovery section. The temperature of the flue gas from the burner should be recorded.
3. A test unit of the CHE may be built based on the geometry and materials of construction presented in this work. For flue gas conditions different from the ones presented here, or if the client specifications for the oil or the dimensions of the CHE need to be changed, the heat transfer model may easily be used to calculate the new area for heat transfer.
4. The control unit should be sized according to the predicted maximum flue gas flow rate and the flue gas temperature. This will determine the amount of heat to be removed from the oil stream before it enters the client unit.
5. For the test unit, measuring the flue gas velocity in the middle of the CHE and in the gap between the coiled tube and the stack, will improve the estimates of the Reynolds number used in the correlations of the convective heat transfer coefficients h_{co} and h_{si}.
6. The amount of electricity from the Organic Rankine Cycle is too small to export it to the existing electrical grid (if present) and should ideally be used locally to power the burner components or other devices at the battery site.

7. If the maintenance of the Organic Rankine Cycle is high or its operation requires frequent supervision, simpler applications for the hot oil stream may be in "treater" vessels (where crude oil is separated from water), or space heating at the battery site.

8. A dynamic study should also be performed to evaluate the performance of the heat recovery system and its control system under varying operating conditions.

References

Alberta Energy and Utilities Board (AEUB), "Guide 60: Upstream Petroleum Industry Flaring Guide", Alberta Energy and Utilities Board Guide Series, (1999).

Alberta Energy and Utilities Board (AEUB), "Upstream Petroleum Industry Flaring and Venting Report, 2003", Statistical Series (ST) 2004-60B, (2004).

Brzustowski, T. A., "Flaring in the Energy Industry", Progress in Energy and Combustion Science **2**, 129–141 (1976).

Bussman, W., J. Franklin and R. Schwartz, "Corrosion of Flare Tips". In: "Corrosion 1997, Proceedings of the NACE International's Annual Conference", Chicago (1997).

Edwards, L. and M. Endean (eds.), "Manufacturing with Materials", Butterworth-Heinemann, Oxford, (1995).

Extol Industrial Insulation, "Data Sheet for Sproule® Perlite Insulation", Extol of Ohio Inc., 208 Republic Street, Norwalk, Ohio 44857, in http://www.extolohio.com, 27 February 2004.

Gogolek, P. E. G. and A. C. S. Hayden, "Efficiency of Flare Flames in Turbulent Crosswind", American Flame Research Committee (AFRC) 2002 Spring Meeting, Ottawa, ON, May 8-10 (2002).

Himmelblau, D. M. and J. B. Riggs, "Basic Principles and Calculations in Chemical Engineering", Prentice Hall, New Jersey (2004).

Holford M. R. and J. P. Hettiaratchi, "An Evaluation of Potential Technologies for Reducing Solution Gas Flaring in Alberta", Report to the Clean Air Strategic Alliance (CASA) Flaring Project Team, University of Calgary, Calgary, Alberta (1998).

Hottel, H. C. and A. F. Sarofim, "Radiative Transfer", McGraw-Hill, New York (1967).

Intergovernmental Panel on Climate Change (IPCC), "Climate Change 2001: The Scientific Basis", §6, in http://www.ipcc.ch/, (2001).

Johnson, M. R., J. L. Spangelo and L. W. Kostiuk, "A Characterization of Solution Gas Flaring in Alberta", Journal of the Air & Waste Management Association **51**, 1167–1177 (2001).

Johnson, M. R. and L. W. Kostiuk, "A Parametric Model for the Efficiency of a Flare in Crosswind", Proceedings of the Combustion Institute **29**, 1943–1950 (2002).

MatWeb Material Property Data, "AISI Type 310 Stainless Steel, Annealed Plate", in http://matweb.com/search/SpecificMaterial.asp?bassnum=Q310C, 24 March 2004.

Mills, A. F., "Heat Transfer", Prentice Hall, New Jersey (1999).

Mori, Y., K. Watanabe and T. Taira, "Radiation Effects on Heat Transfer in Heat Exchangers", Journal of the Japan Society of Mechanical Engineers, **46**, 1523–1533 (1980).

Perry, R. H. and D.W. Green (eds.), "Perry's Chemical Engineers' Handbook", McGraw-Hill, New York (1997).

Shah, R.K. and S.D. Joshi, "Convective Heat Transfer in Curved Ducts". In: Kakaç, S., R.K. Shah and W. Aung (eds.), "Handbook of Single-Phase Convective Heat Transfer", John Wiley & Sons, New York (1987).

Smith, J.M., H.C. Van Ness and M.M. Abbott, "Introduction to Chemical Engineering Thermodynamics", McGraw-Hill, New York (1996).

Solutia Inc., "Therminol®59 Technical Bulletin 7239271", Solutia Inc., St. Louis, Missouri, P.O. Box 66760, (1995).

Unifrax Corp., "Fiberfrax® Blanket and Mat Products, Form C-1421", Unifrax Corporation, 2351 Whirlpool Street, Niagara Falls, New York 14305-2413 (2002).

Appendix A. CD ROM Contents

The contents of the CD ROM are as follows:

Combustion Calculations spreadsheet

The Combustion Calculations spreadsheet was developed in Excel to analyse the complete combustion of multi-component gaseous fuels (natural and synthetic gases) under the same assumptions as in the reference case (see §2.1.1). Three pieces of information are required in Combustion Calculations (under worksheet "Combustion"):

1) the stoichiometric number ($\lambda_A \geq 1$),
2) the fuel mass flow rate (kg/s) and,
3) the fuel composition in terms of mole fractions. Possible components are: methane, ethane, ethene, propane, n-butane, carbon monoxide, hydrogen gas, carbon dioxide, nitrogen and oxygen.

The spreadsheet then calculates:

1) the molar (kmol/s), mass (kg/s) and volumetric (m^3/s) amounts of combustion air,
2) the air-to-fuel mass ratio,
3) the molar (kmol/s) and volumetric (m^3/s) amounts and molar fractions of combustion products (carbon dioxide, water vapour and excess oxygen and inert nitrogen).

Building on the ability of Combustion Calculations to determine the flue gas composition for a multi-component fuel stream, two tables were added on worksheet "TFT" to calculate the enthalpy of reactants and products. The molar flow rates are taken automatically from the first worksheet ("Combustion"). The user can set the inlet temperature of each component and may give an educated guess for the outlet temperature. The theoretical flame temperature is obtained by using the Goal Seek function (under the drop-down menu "Tools") to minimise the value of $\Delta H_{out} - \Delta H_{in}$ by modifying T_{out}. The theoretical flame temperature is reported on the last line.

CHE Simulator spreadsheet

Programmed in Microsoft Visual Basic behind an Excel spreadsheet, CHE Simulator can be readily customised. Values in bold (ambient air temperature, flow rate of oil, etc.) on the first row of the simulator may be changed according to the conditions that need to be tested. Comments have been added to some cells to clarify their meaning further and units are clearly stated. The basis of the CV has been set to one full turn of coiled tube ($\Delta x = l_{turn}$) and its value may be modified from the first row as well. In order to change the geometry of the CHE or the heat transfer correlations, one may access the Visual Basic Editor by pressing Alt-F11. The code is contained in the module "Code_CHE_Simulator" and has been extensively documented to facilitate interpretation.

To carry out the design calculation, specify a guessed value of the temperature of the flue gas leaving the first CV (= first cell underneath cell "Tf_iPlus1"). This initial guess may be calculated from an energy balance on the flue gas stream knowing the flue gas temperature at the bottom of the CHE and assuming that $Q_{flue} \approx 1.1 Q_{oil}$ to account for heat losses. By adding successive CV (rows in the spreadsheet), track the value of "Toi" (the oil temperature leaving the i^{th} CV) until it reaches the desired value (e.g., 180°C in the reference case). Then check the flue gas temperature on the last CV. If it is close (< 5°C) to the known flue gas temperature at the bottom of the CHE, the simulation has converged properly. The outside surface area of the coiled tube, its length and the number of turns of the CHE appear at the beginning of the last CV added. If the difference in flue gas temperature is large, adjust the initial guess of the temperature of the flue gas leaving the first CV, until the last flue gas temperature matches the known value. It is possible that two slightly different combinations of the number of CV plus the flue gas temperature leaving the first CV (first cell underneath cell "Tf_iPlus1") yield results which are close but not identical. For example, when solving for the area of the coiled tube needed to raise the temperature of the 0.5828 kg/s oil stream from 123.4°C to 180°C with 0.2614 kg/s of flue gas entering at 800°C in SUMMER conditions (T_e = 30°C, h_{so} = 10 W/m^2°C), two solutions are found:

$T_{f,1}$ = 582°C and N = 32 → $T_{f,N+1}$ = 802.3°C; $T_{o,N}$ = 179.1°C; $T_{s1,N}$ = 664.5°C

$T_{f,1}$ = 575°C and N = 33 → $T_{f,N+1}$ = 799.6°C; $T_{o,N}$ = 180.1°C; $T_{s1,N}$ = 662.5°C

In this case it seems more appropriate to choose the second one since $T_{o,N}$ is closer to the 180°C target and the $T_{f,N+1}$ are fairly close. Thus, some judgment is necessary in the design calculation. However with a reasonable estimate of $T_{f,1}$, discrepancies will be likely over one turn of the coiled tube more or less.

The performance scenario is simpler to execute since the number of CV (rows) is already known (A_{co} and number of turns N are fixed). Set as many rows of the simulator as there are CV to match the known number of turns. Provide a guess for the flue gas temperature at the top of the CHE (CV = 0) as in the design scenario. Set "Toi" to the known value. Check the flue gas temperature on the last CV. If it is close (< 5°C) to the known flue gas temperature at the bottom of the CHE, the simulation has converged properly. The oil temperature at the bottom of the CHE appears on the row of the last CV. If the difference in flue gas temperature is large, adjust the initial guess of the temperature of the flue gas leaving the first CV, until the last flue gas temperature matches the known value. Since the variable of interest in the performance scenario is the oil temperature given a fixed number of CV and the flue gas temperature at the bottom of the CHE, there is only one possible solution (and not two as in the design scenario).

Materials of Construction Data

Thermal conductivity data for insulating material Durablanket S® (personal communication with Unifrax Corp., 2004).

Appendix B. Solution of the Reference Case

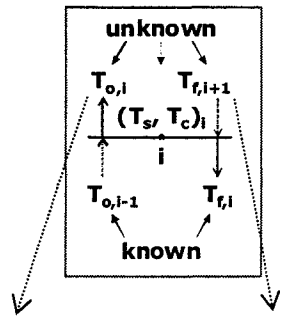

CHE Simulator – Counter-current configuration

To add one more CV (design problem), highlight the last row and drag it down one line
The figures on each row are the final results for that CV
Variable names correspond to those used in actual code

CV	L	Aco	No. turns	Te	hso	thick_ins	mfr_oil	mfr_flue	Δx	Toi	ΔToi	Tf_iPlus1
	m	m^2		°C	W/m^2K	m	kg/s	kg/s	m	°C	°C	°C
0	0	0	0	**-30**	**60**	**0.0127**	**0.5828**	**0.1307**	**0.5360**	**123.4**	**1**	**867**
1	0.536	0.056	1.0	-30	60	0.0127	0.5828	0.1307	0.5360	125.506	2.106	882.693
2	1.072	0.112	2.0	-30	60	0.0127	0.5828	0.1307	0.5360	127.663	2.157	898.776
3	1.608	0.169	3.0	-30	60	0.0127	0.5828	0.1307	0.5360	129.872	2.209	915.263
4	2.144	0.225	4.0	-30	60	0.0127	0.5828	0.1307	0.5360	132.135	2.263	932.168
5	2.680	0.281	5.0	-30	60	0.0127	0.5828	0.1307	0.5360	134.454	2.319	949.506
6	3.216	0.337	6.0	-30	60	0.0127	0.5828	0.1307	0.5360	136.830	2.376	967.293
7	3.752	0.394	7.0	-30	60	0.0127	0.5828	0.1307	0.5360	139.266	2.436	985.544
8	4.288	0.450	8.0	-30	60	0.0127	0.5828	0.1307	0.5360	141.764	2.498	1004.276
9	4.824	0.506	9.0	-30	60	0.0127	0.5828	0.1307	0.5360	144.326	2.562	1023.508
10	5.360	0.562	10.0	-30	60	0.0127	0.5828	0.1307	0.5360	146.954	2.628	1043.258
11	5.896	0.619	11.0	-30	60	0.0127	0.5828	0.1307	0.5360	149.650	2.697	1063.545
12	6.431	0.675	12.0	-30	60	0.0127	0.5828	0.1307	0.5360	152.418	2.768	1084.390
13	6.967	0.731	13.0	-30	60	0.0127	0.5828	0.1307	0.5360	155.260	2.842	1105.813
14	7.503	0.787	14.0	-30	60	0.0127	0.5828	0.1307	0.5360	158.178	2.918	1127.837
15	8.039	0.844	15.0	-30	60	0.0127	0.5828	0.1307	0.5360	161.175	2.997	1150.484
16	8.575	0.900	16.0	-30	60	0.0127	0.5828	0.1307	0.5360	164.255	3.080	1173.780
17	9.111	0.956	17.0	-30	60	0.0127	0.5828	0.1307	0.5360	167.420	3.165	1197.749
18	9.647	1.012	18.0	-30	60	0.0127	0.5828	0.1307	0.5360	170.673	3.254	1222.417
19	10.183	1.069	19.0	-30	60	0.0127	0.5828	0.1307	0.5360	174.019	3.345	1247.812
20	10.719	1.125	20.0	-30	60	0.0127	0.5828	0.1307	0.5360	177.460	3.441	1273.963
21	11.255	1.181	21.0	-30	60	0.0127	0.5828	0.1307	0.5360	181.000	3.540	1300.898

CV	Tc1 °C	Tc2 °C	Ts1 °C	Ts2 °C	Ts3 °C	Ts4 °C	Num. Iter	hco W/m²K	hrc W/m²K	hsi W/m²K	hci W/m²K
0	**123.4**	**168**	**500**	**490**	**20**	**18**					
1	150.697	164.554	612.949	611.733	29.264	29.192	5	44.780	17.966	16.368	2300.75
2	153.231	167.440	622.269	621.027	30.848	30.774	4	44.942	18.386	16.394	2329.56
3	155.825	170.397	631.771	630.504	32.488	32.413	4	45.108	18.818	16.422	2359.22
4	158.481	173.430	641.440	640.145	34.195	34.117	4	45.277	19.264	16.450	2389.73
5	161.201	176.541	651.277	649.954	35.969	35.889	4	45.450	19.725	16.479	2421.13
6	163.989	179.733	661.286	659.934	37.815	37.733	4	45.627	20.200	16.509	2453.43
7	166.845	183.009	671.469	670.087	39.736	39.651	4	45.808	20.690	16.541	2486.64
8	169.774	186.373	681.829	680.416	41.735	41.648	4	45.993	21.197	16.573	2520.79
9	172.778	189.829	692.369	690.924	43.816	43.727	4	46.182	21.719	16.606	2555.88
10	175.860	193.379	703.091	701.612	45.984	45.892	4	46.377	22.259	16.639	2591.92
11	179.022	197.028	713.997	712.484	48.242	48.147	4	46.575	22.816	16.674	2628.93
12	182.269	200.780	725.088	723.540	50.594	50.497	4	46.779	23.391	16.708	2666.91
13	185.603	204.639	736.367	734.782	53.045	52.944	4	46.987	23.985	16.743	2705.84
14	189.028	208.609	747.874	746.251	55.589	55.485	5	47.201	24.597	16.778	2745.75
15	192.549	212.696	759.534	757.871	58.248	58.141	5	47.420	25.230	16.813	2786.59
16	196.169	216.905	771.383	769.678	61.019	60.909	5	47.645	25.883	16.846	2828.35
17	199.893	221.242	783.418	781.671	63.906	63.792	5	47.875	26.557	16.879	2871.01
18	203.725	225.711	795.638	793.847	66.912	66.795	5	48.112	27.253	16.911	2914.54
19	207.670	230.319	808.039	806.203	70.043	69.922	5	48.354	27.970	16.940	2958.90
20	211.733	235.071	820.616	818.733	73.302	73.177	5	48.603	28.711	16.967	3004.04
21	215.920	239.975	833.362	831.430	76.692	76.562	5	48.858	29.474	16.991	3049.90

CV	R_hco K/W	R_hrc K/W	R_hsi K/W	R_s K/W	R_ins K/W	R_jack K/W	R_hso K/W	R_c K/W	R_hci K/W	R_fc K/W	R_fs K/W	R_stack K/W	R_coil K/W
1	0.3971	0.9897	1.302	0.006	2.985	0.0004	0.303	0.006	0.010	0.2834	1.3021	3.2953	0.016
2	0.3957	0.9671	1.300	0.006	2.946	0.0004	0.303	0.006	0.010	0.2808	1.3000	3.2560	0.016
3	0.3942	0.9449	1.298	0.006	2.907	0.0004	0.303	0.006	0.010	0.2782	1.2979	3.2167	0.015
4	0.3927	0.9230	1.296	0.006	2.867	0.0004	0.303	0.006	0.010	0.2755	1.2956	3.1770	0.015
5	0.3912	0.9015	1.293	0.006	2.827	0.0004	0.303	0.006	0.010	0.2728	1.2933	3.1368	0.015
6	0.3897	0.8803	1.291	0.006	2.786	0.0004	0.303	0.006	0.010	0.2701	1.2909	3.0963	0.015
7	0.3882	0.8594	1.289	0.006	2.746	0.0004	0.303	0.006	0.009	0.2674	1.2885	3.0553	0.015
8	0.3866	0.8389	1.286	0.006	2.704	0.0004	0.303	0.005	0.009	0.2647	1.2860	3.0141	0.015
9	0.3850	0.8187	1.283	0.006	2.663	0.0004	0.303	0.005	0.009	0.2619	1.2835	2.9724	0.015
10	0.3834	0.7989	1.281	0.006	2.621	0.0004	0.303	0.005	0.009	0.2591	1.2809	2.9305	0.014
11	0.3818	0.7794	1.278	0.006	2.579	0.0004	0.303	0.005	0.009	0.2563	1.2782	2.8883	0.014
12	0.3801	0.7602	1.276	0.006	2.536	0.0004	0.303	0.005	0.009	0.2534	1.2756	2.8458	0.014
13	0.3784	0.7414	1.273	0.006	2.494	0.0004	0.303	0.005	0.009	0.2505	1.2729	2.8031	0.014
14	0.3767	0.7229	1.270	0.006	2.451	0.0004	0.303	0.005	0.009	0.2477	1.2703	2.7606	0.014
15	0.3750	0.7048	1.268	0.006	2.408	0.0004	0.303	0.005	0.008	0.2448	1.2677	2.7175	0.014
16	0.3732	0.6870	1.265	0.006	2.365	0.0004	0.303	0.005	0.008	0.2418	1.2651	2.6743	0.014
17	0.3714	0.6696	1.263	0.006	2.322	0.0004	0.303	0.005	0.008	0.2389	1.2626	2.6310	0.013
18	0.3696	0.6525	1.260	0.006	2.278	0.0004	0.303	0.005	0.008	0.2359	1.2603	2.5877	0.013
19	0.3677	0.6357	1.258	0.006	2.235	0.0004	0.303	0.005	0.008	0.2330	1.2581	2.5444	0.013
20	0.3659	0.6193	1.256	0.006	2.192	0.0004	0.303	0.005	0.008	0.2300	1.2561	2.5011	0.013
21	0.3639	0.6033	1.254	0.005	2.149	0.000	0.303	0.005	0.008	0.227	1.2544	2.4579	0.013

CV	Q_oil W	Q_loss W	Q_flue W	Q_conv W	Q_rad W	Re_co	Pr_co	Re_si	Pr_si	Re_ci	Pr_ci	var_prop
1	2478.71	-195.11	-2673.82	1768.97	709.74	2768.5	0.74	14241.9	0.80	30086.1	17.47	1.030
2	2547.30	-200.33	-2747.63	1807.74	739.56	2731.2	0.74	14058.6	0.80	30792.2	17.17	1.030
3	2618.54	-205.73	-2824.27	1847.70	770.84	2694.1	0.74	13877.3	0.80	31530.9	16.86	1.030
4	2692.58	-211.34	-2903.93	1888.89	803.69	2657.2	0.74	13697.9	0.81	32304.2	16.56	1.031
5	2769.56	-217.19	-2986.75	1931.37	838.20	2620.6	0.74	13520.4	0.81	33113.7	16.25	1.031
6	2849.64	-223.26	-3072.91	1975.18	874.46	2584.1	0.74	13344.8	0.82	33961.6	15.94	1.031
7	2932.97	-229.59	-3162.56	2020.40	912.57	2547.9	0.74	13171.0	0.82	34850.0	15.63	1.032
8	3019.72	-236.17	-3255.89	2067.07	952.65	2512.0	0.74	12998.9	0.83	35781.0	15.32	1.032
9	3110.07	-243.02	-3353.09	2115.27	994.80	2476.3	0.74	12828.5	0.83	36756.8	15.01	1.032
10	3204.21	-250.16	-3454.36	2165.06	1039.15	2440.8	0.75	12659.7	0.84	37780.0	14.71	1.032
11	3302.32	-257.59	-3559.92	2216.51	1085.82	2405.6	0.75	12492.4	0.85	38852.8	14.40	1.033
12	3404.64	-265.34	-3669.97	2269.70	1134.94	2370.7	0.75	12326.4	0.85	39977.9	14.09	1.033
13	3511.36	-273.40	-3784.77	2324.70	1186.66	2336.0	0.75	12161.7	0.86	41157.7	13.79	1.033
14	3622.69	-281.78	-3904.47	2381.60	1241.08	2301.6	0.75	11998.2	0.87	42394.9	13.48	1.033
15	3738.95	-290.54	-4029.49	2440.49	1298.46	2267.5	0.76	11835.5	0.87	43691.9	13.18	1.033
16	3860.37	-299.66	-4160.03	2501.46	1358.92	2233.7	0.76	11673.6	0.88	45051.3	12.88	1.033
17	3987.22	-309.16	-4296.38	2564.60	1422.62	2200.1	0.76	11512.3	0.89	46475.6	12.59	1.033
18	4119.79	-319.06	-4438.85	2630.02	1489.77	2166.9	0.76	11351.2	0.90	47967.2	12.30	1.033
19	4258.37	-329.37	-4587.74	2697.82	1560.56	2134.0	0.77	11190.2	0.91	49528.2	12.01	1.033
20	4403.29	-340.10	-4743.39	2768.11	1635.18	2101.4	0.77	11028.8	0.92	51160.5	11.73	1.033
21	4554.88	-351.26	-4906.13	2841.02	1713.86	2069.2	0.77	10866.8	0.93	52866.0	11.45	1.032

CV	T_c_avg °C	T_s_avg °C	T_ins_avg °C	T_jack_avg °C	tauTs1	tauTc2	eps_fc	alp_Tc2	alp_Ts1	Js W/m^2	Jc W/m^2	Gc W/m^2
1	157.626	612.341	320.499	29.228	0.923	0.831	0.057	0.169	0.077	23670.84	14701.58	27321.95
2	160.335	621.648	325.937	30.811	0.924	0.832	0.056	0.168	0.076	24632.80	15287.28	28438.01
3	163.111	631.138	331.496	32.451	0.925	0.834	0.055	0.166	0.075	25641.69	15901.43	29608.36
4	165.955	640.792	337.170	34.156	0.926	0.835	0.054	0.165	0.074	26701.02	16546.17	30837.22
5	168.871	650.616	342.962	35.929	0.927	0.837	0.053	0.163	0.073	27813.71	17223.27	32127.92
6	171.861	660.610	348.874	37.774	0.928	0.838	0.052	0.162	0.072	28982.82	17934.60	33484.04
7	174.927	670.778	354.911	39.693	0.929	0.839	0.051	0.161	0.071	30211.62	18682.13	34909.34
8	178.074	681.122	361.075	41.691	0.930	0.841	0.050	0.159	0.070	31503.60	19467.99	36407.84
9	181.303	691.646	367.370	43.772	0.931	0.842	0.049	0.158	0.069	32862.43	20294.42	37983.8
10	184.619	702.351	373.798	45.938	0.932	0.844	0.048	0.156	0.068	34292.03	21163.80	39641.74
11	188.025	713.240	380.363	48.195	0.933	0.845	0.047	0.155	0.067	35796.56	22078.67	41386.45
12	191.524	724.314	387.067	50.545	0.934	0.847	0.046	0.153	0.066	37380.44	23041.70	43223.03
13	195.121	735.575	393.913	52.994	0.935	0.849	0.045	0.151	0.065	39048.34	24055.77	45156.86
14	198.818	747.062	400.920	55.537	0.936	0.850	0.044	0.150	0.064	40803.60	25122.90	47191.56
15	202.623	758.703	408.060	58.195	0.937	0.852	0.043	0.148	0.063	42654.47	26248.15	49337.07
16	206.537	770.530	415.349	60.964	0.938	0.853	0.042	0.147	0.062	44605.08	27434.04	51597.93
17	210.567	782.545	422.788	63.849	0.939	0.855	0.041	0.145	0.061	46661.31	28684.17	53980.9
18	214.718	794.743	430.380	66.854	0.940	0.857	0.040	0.143	0.060	48829.34	30002.34	56493.08
19	218.994	807.121	438.123	69.983	0.941	0.858	0.039	0.142	0.059	51115.67	31392.55	59141.94
20	223.402	819.675	446.017	73.239	0.942	0.860	0.038	0.140	0.058	53527.18	32859.01	61935.34
21	227.947	832.396	454.061	76.627	0.943	0.862	0.037	0.138	0.057	56071.01	34406.15	64881.49